

P-wave excited baryons from pion- and photo-induced hyperon production

A.V. Anisovich^{1,2}, E. Klempt¹, V.A. Nikonov^{1,2}, A.V. Sarantsev^{1,2} and U. Thoma¹

¹ Helmholtz-Institut für Strahlen- und Kernphysik, Universität Bonn, Germany

² Petersburg Nuclear Physics Institute, Gatchina, Russia

Received: October 29, 2010/ Revised version:

Abstract. We report evidence for $N(1710)P_{11}$, $N(1875)P_{11}$, $N(1900)P_{13}$, $\Delta(1600)P_{33}$, $\Delta(1910)P_{31}$, and $\Delta(1920)P_{33}$, and find indications that $N(1900)P_{13}$ might have a companion state at 1970 MeV. The controversial $\Delta(1750)P_{31}$ is not seen. The evidence is derived from a study of data on pion- and photo-induced hyperon production, but other data are included as well. Most of the resonances reported here were found in the Karlsruhe-Helsinki (KH84) [1] and the Carnegie-Mellon (CM) [2] analyses but were challenged recently by the Data Analysis Center at GWU [3]. Our analysis is constrained by the energy independent πN scattering amplitudes from either KH84 or GWU. The two πN amplitudes from KH84 or GWU, respectively, lead to slightly different πN branching ratios of contributing resonances but the debated resonances are required in both series of fits.

PACS: 11.80.Et, 11.80.Gw, 13.30.-a, 13.30.Ce, 13.30.Eg, 13.60.Le 14.20.Gk

1 Introduction

The existence of radially excited resonances and - if affirmed - their mass pattern represents one of the most controversial issues in baryon spectroscopy (see, e.g., [4] for a recent review). Well known is the problem of the lowest mass nucleon excitation $N(1440)P_{11}$, the so-called Roper resonance [5]. It is studied in many reactions, and its existence is beyond doubt. But its - compared to quark model calculations - low mass and its broad width has invited speculations that it could be dynamically generated and unrelated to (qqq) spectroscopy. In the P_{11} -wave, discrepancies between different analyses show up above the Roper resonance. Höhler and collaborators [1] and Cutkosky and collaborators [2] identified two further states in the P_{11} partial wave, $N(1710)P_{11}$ and $N(2100)P_{11}$. Manley and Saleski [6] found two resonances as well, $N(1710)P_{11}$ and a state at 1885 MeV (listed under the $N(2100)P_{11}$ PDG entry [7]) which is confirmed in a coupled channel analysis of photo-production data [8] but not listed in the PDG listing as separate state. In [9], observation of $N(1710)P_{11}$ and $N(2100)P_{11}$ was reported. Hence there seem to be two or possibly even three P_{11} states with spin-parity $J^P = 1/2^+$ above the Roper resonance. However, in a recent analysis of a large body of πN elastic and charge exchange scattering data, only the Roper resonance was confirmed [3] putting into doubt the existence of the three candidate resonances above it. The authors in [10] suggest that the two lowest P_{11} nucleon resonances, the Roper

$N(1440)P_{11}$ and $N(1710)P_{11}$, originate from a single bare state. In the P_{13} wave, the existence of $N(1720)P_{13}$ is beyond doubt (even though not seen in [10]) but the next state, $N(1900)P_{13}$, was observed in none of the πN amplitude analyses [1,2,3] but only in coupled channel analyses [6,11,176] which included some inelastic channels.

A similar situation is found for Δ excitations. In [3], the lowest-mass resonance above $\Delta(1232)P_{33}$, the $\Delta(1600)P_{33}$ resonance, is found with a much larger width than reported in analyses of elastic scattering data [1,2,6] and of inelastic reactions [6,176,13]. The $\Delta(1920)P_{33}$ resonance is absent in [3]. To complete the low-spin positive-parity states, we mention $\Delta(1750)P_{31}$ which is seen in some inelastic reactions [6,9,176] and not seen in the analyses of [1,2]. In [3], one pole is found in the P_{31} wave at $(M, \Gamma) = (1771, 479)$ MeV which is consistent with $\Delta(1750)P_{31}$. A Breit-Wigner resonance yields $M = 2067.9 \pm 1.7$ MeV and $\Gamma = 543 \pm 10$ MeV. The four-star $\Delta(1910)P_{31}$ is argued to be highly questionable. In [10], the 3-star $\Delta(1600)P_{33}$ and the two 4-star resonances $\Delta(1910)P_{31}$ and $\Delta(1920)P_{33}$ are all missing.

The situation is thus very unsatisfactory. The Particle Data Group bases the evidence for the existence of states nearly entirely on four analyses [1,2,3,6]. The latest analysis by Arndt *et al.* [3] includes high precision data from the meson factories at LAMPF, PSI, and TRIUMF which constrain the low-energy region very precisely, and important measurements of spin rotation parameters (see [3] for a list of data). Hence one should expect that the analysis [3] should also be the most reliable one. But this analysis challenges the existence of many resonances. A strong argument in favor of the Arndt analysis is the correct prediction of spin rotation parameters [14,15,16] and of the backward asymmetry [17] in the elastic pion-proton scattering

Correspondence to: klempt@hiskp.uni-bonn.de

The πN induced amplitudes, photoproduction observables and multipoles for both solutions (BG2010-01 and 02) can be downloaded from our web site as figures or in the numerical form (<http://pwa.hiskp.uni-bonn.de>).

from ITEP/PNPI while the predictions from [1,2] show clear discrepancies with the data. On the other hand, it is difficult to believe that the consistency between the older analyses is just fortuitous.

A difficulty in the partial wave analysis of πN elastic scattering data lies in the fact that the amplitudes cannot be constructed from the data on πN elastic (and charge exchange) scattering without theoretical input. For most energies and most angles, only the differential cross section $d\sigma/d\Omega$ and the target asymmetry (describing the distribution of the angle between scattering plane and target polarization) are known. From this data, the absolute values of the spin-flip and spin non-flip amplitudes $|H|$ and $|G|$ can be determined but not their phases. This continuum ambiguity can only be resolved by enforcing dispersion relations. Likely, the different use of dispersion relations is responsible for the differences between the old analyses of [1,2] and the analysis presented in [3].

In this paper we study the consistency of the $\pi N \rightarrow \pi N$ scattering amplitudes for low-spin positive-parity resonances from the analyses [1,3] with the πN and γN transition amplitudes into kaon-hyperon and ηN final states:

$$\pi^- p \rightarrow \Lambda K^0 \quad (1a)$$

$$\pi^+ p \rightarrow \Sigma^+ K^+ \quad (1b)$$

$$\pi^- p \rightarrow \Sigma^0 K^0 \quad (1c)$$

$$\text{and } \pi^- p \rightarrow \Lambda \begin{matrix} n \eta \\ \gamma p \end{matrix} \quad (1d) \quad (2a)$$

$$\gamma p \rightarrow \Sigma^0 K^+ \quad (2b)$$

$$\gamma p \rightarrow \Sigma^+ K^0 \quad (2c)$$

$$\gamma p \rightarrow p \pi^0 \quad (2d)$$

$$\gamma p \rightarrow p \eta \quad (2e)$$

The study of strangeness production has a few distinctive advantages. The differential cross sections for these reactions are known with reasonable accuracy and, due to the self-analyzing power of the final-state hyperons, the recoil polarization can be determined from the hyperon decay. Reactions (1a, 1d, 2a, 2e) are restricted to nucleon resonances, reaction (1b) to Δ resonances, reactions (1c, 2b, 2c) receive contributions from both. Hence the isospin decomposition of the transition amplitude is defined by the data.

Here we use, alternatively, the energy independent elastic πN amplitudes from [1] or [3], respectively, to find energy dependent amplitudes satisfying the data on elastic scattering and on reactions (1a)-(2e). In addition, the amplitudes are constrained by a large number of photoproduction data. The Cutkosky amplitudes [2] are mostly in between the Arndt and the Höller amplitudes. We did not use these systematically since we did not expect additional insight.

The use of a large number of final states constrains the inelasticity of the πN amplitude which otherwise is a free fit parameter to be determined for every bin. This is a major advantage of this analysis compared to those of [1,2,3]. A major result of this analysis is that the existence and the properties of all resonances used here are hardly affected by the choice of elastic πN amplitudes [1,3]. Only the πN coupling constants of resonances change, and even this change is moderate. We account for the difference by increasing the error in the πN branching ratios.

Finally, we comment on the naming scheme we adopt. We use the conventional names of the Particle Data Group [7]: $N(\text{mass})L_{2I,2J}$ and $\Delta(\text{mass})L_{2I,2J}$ where I and J are isospin and total spin of the resonance and L the orbital angular momentum in the decay of the resonance into nucleon and pion. For resonances not included in [7], we use $N_{JP}(\text{mass})$ and $\Delta_{JP}(\text{mass})$ which gives the spin-parity of the resonance. The latter scheme is adopted from the meson naming scheme and easily understood also outside of the baryon community. In this way, the reader can easily see which resonances are introduced here and which resonances found here are compatible with PDG values.

2 Data, PWA method, and fits

2.1 Data

Tables 1-5 summarize the data used here. Given are the reaction, the observables and references to the data, the number of data points, the weight with which the data are used in the fits, and the χ^2 per data point of our final solution BG2010-02.

Table 1. Pion induced reactions fitted in the coupled-channel analysis and χ^2 contributions for the solution BG2010-02.

$\pi N \rightarrow \pi N$	Wave	N_{data}	w_i	χ_i^2/N_{data}
[3]	S_{11}	104	30	1.95
	S_{31}	112	20	2.07
	P_{11}	112	50	2.12
	P_{31}	104	20	3.86
	P_{13}	112	25	1.22
	P_{33}	120	15	2.87
	D_{13}	96	10	2.87
	D_{33}	108	12	2.68
	D_{15}	96	20	3.67
	F_{35}	62	20	1.48
	F_{37}	72	10	2.76
$\pi^- p \rightarrow \eta n$	Observ.	N_{data}	w_i	χ_i^2/N_{data}
[18]	$d\sigma/d\Omega$	68	20	1.68
[19]	$d\sigma/d\Omega$	84	30	2.50
$\pi^- p \rightarrow K^0 \Lambda$	Observ.	N_{data}	w_i	χ_i^2/N_{data}
[20]	$d\sigma/d\Omega$	298	30	2.31
[21,22]	$d\sigma/d\Omega$	299	30	0.90
[21,22]	P	354	30	1.98
[23]	β	72	100	2.45
$\pi^+ p \rightarrow K^+ \Sigma^+$	Observ.	N_{data}	w_i	χ_i^2/N_{data}
[24]	$d\sigma/d\Omega$	609	35	1.27
[24]	P	304	30	1.58
[25]	β	7	1000	1.97
$\pi^- p \rightarrow K^0 \Sigma^0$	Observ.	N_{data}	w_i	χ_i^2/N_{data}
[26]	$d\sigma/d\Omega$	259	30	0.77
[26]	P	90	30	1.36

Table 2. Reactions leading to 3-body final states are included in event-based likelihood fits for the solution BG2010-02. CB stands for CB-ELSA; CBT for CBELSA/TAPS.

$d\sigma/d\Omega(\pi^- p \rightarrow \pi^0 \pi^0 n)$	N_{data}	w_i	$-\ln L$
T=373 MeV	5248	10	-939
T=472 MeV	Crystal	5	-2605
T=551 MeV	Ball [27]	2.5	-7245
T=655 MeV	(BNL)	2	-14926
T=691 MeV		3.5	-8055
T=748 MeV		4	-6952
$d\sigma/d\Omega(\gamma p \rightarrow \pi^0 \pi^0 p)$ CB [28,29]	110601	4	-26795
$d\sigma/d\Omega(\gamma p \rightarrow \pi^0 \eta p)$ CB [13,30,31]	17468	8	-5652
	N_{data}	w_i	χ^2/N_{data}
$\Sigma(\gamma p \rightarrow \pi^0 \pi^0 p)$ GRAAL [32]	128	35	0.96
$\Sigma(\gamma p \rightarrow \pi^0 \eta p)$ CBT [33]	180	15	2.41
$E(\gamma p \rightarrow \pi^0 \pi^0 p)$ GDH/A2 [34]	16	35	1.31

Table 3. Observables from π photoproduction fitted in the coupled-channel analysis and χ^2 contributions for the solution BG2010-02.

$\gamma p \rightarrow \pi^0 p$	Observ.	N_{data}	w_i	χ^2/N_{data}
[35] (TAPS@MAMI)	$d\sigma/d\Omega$	1691	0.8	1.81
[36,37] (GDH A2)	$d\sigma/d\Omega$	164	7	1.17
[38] (GRAAL)	$d\sigma/d\Omega$	861	2	1.59
[39,40] (CB)	$d\sigma/d\Omega$	1106	3.5	1.65
[41] (CLAS)	$d\sigma/d\Omega$	592	6	1.81
[38,42,43,44,45,46,47,48,49](GRAAL a.o.)	Σ	1492	3	2.82
[50] (CBT)	Σ	374	30	1.03
[43,44,45,51,52,53,54,55,56,57,58,59,60]	T	389	8	3.16
[43,44,45,60,61,62,63,64]	P	607	5	1.20
[65,66]	G	75	5	1.51
[65]	H	71	5	1.51
[36,37]	E	140	7	1.30
[63,67]	O_x	7	10	0.95
[63,67]	O_z	7	10	0.42
$\gamma p \rightarrow \pi^+ n$	Observ.	N_{data}	w_i	χ^2/N_{data}
[68,69,70,71,72,73,74,75,76,77,78,79]	$d\sigma/d\Omega$	1583	14	1.75
[37,80] (GDH A2)	$d\sigma/d\Omega$	408	14	0.55
[81] (CLAS)	$d\sigma/d\Omega$	484	4	1.54
[49,82,83,84,85,86,87,88,89,90,91,92]	Σ	899	3	3.07
[87,88,93,94,95,96,97,98,99,100,101,102,103]	T	661	3	2.66
[87,88,104]	P	252	3	2.41
[66,105,106]	G	86	8	4.97
[105,106,107]	H	128	3	4.59
[37,80]	E	231	14	1.58

Table 4. Observables from η photoproduction fitted in the coupled-channel analysis and χ^2 contributions for the solution BG2010-02.

$\gamma p \rightarrow \eta p$	Observ.	N_{data}	w_i	χ^2/N_{data}
[108] TAPS	$d\sigma/d\Omega$	100	7	2.45
[109] CBT	$d\sigma/d\Omega$	680	40	1.29
[110] GRAAL	Σ	51	10	1.91
[111] GRAAL	Σ	100	15	2.88
[59] PHOENICS	T	50	70	1.29

Table 5. Hyperon photoproduction observables fitted in the coupled-channel analysis and χ^2 contributions for the solution BG2010-02.

$\gamma p \rightarrow K^+ \Lambda$	Observ.	N_{data}	w_i	χ^2/N_{data}
[112] CLAS	$d\sigma/d\Omega$	1320	14	0.81
[113] LEPS	Σ	45	10	3.32
[114] GRAAL	Σ	66	8	1.68
[112] CLAS	P	1270	8	1.90
[114] GRAAL	P	66	10	0.70
[115] GRAAL	T	66	15	1.33
[116] CLAS	C_x	160	15	1.74
[116] CLAS	C_z	159	15	1.45
[115] GRAAL	$O_{x'}$	66	12	1.48
[115] GRAAL	$O_{z'}$	66	15	1.40
$\gamma p \rightarrow K^+ \Sigma$	Observ.	N_{data}	w_i	χ^2/N_{data}
[117] CLAS	$d\sigma/d\Omega$	1280	3.5	1.97
[113] LEPS	Σ	45	10	1.63
[114] GRAAL	Σ	42	10	1.60
[118] CLAS	P	95	10	1.71
[116] CLAS	C_x	94	15	2.89
[116] CLAS	C_z	94	15	1.86
$\gamma p \rightarrow K^0 \Sigma^+$	Obsv.	N_{data}	w_i	χ^2/N_{data}
[118] CLAS	$d\sigma/d\Omega$	48	3	3.25
[119] SAPHIR	$d\sigma/d\Omega$	156	5	1.34
[120] CBT	$d\sigma/d\Omega$	72	10	0.77
[120] CBT	P	72	15	0.95

In the list of πN elastic scattering waves (Table 1), we included the waves F_{35} and F_{37} but not F_{15} and F_{17} . The low-mass part of the F_{15} πN elastic scattering amplitude is easily described by $N(1680)F_{15}$ but the contribution of higher mass states to the pion-induced reactions (1a), (1c), and (1d) is small and ambiguous. The Arndt solution [3] shows more structure than the Höller solution [1] while in most other cases, the Arndt solution is smoother. At the moment, we have no reason to prefer one over the other one. The other partial waves are, however, not affected by this uncertainty. Higher-mass F -wave nucleon resonances do contribute to photoproduction and are included as multichannel relativistic Breit-Wigner amplitudes in the partial-wave analysis of all reactions (1) and (2).

The fit minimizes the total log likelihood defined by

$$-2 \ln \mathcal{L}_{\text{tot}} = \left(\frac{1}{2} \sum w_i \chi_i^2 - \sum w_i \ln \mathcal{L}_i \right) \frac{\sum N_i}{\sum w_i N_i} \quad (3)$$

where the summation over binned data contributes to the χ^2 while unbinned data contribute to the likelihoods \mathcal{L}_i . For convenience of the reader, we quote differences in fit quality as χ^2 difference. $\Delta\chi^2 = -2\Delta\mathcal{L}_{\text{tot}}$. For new data, the weight is increased from $w_i = 1$ until a visually acceptable fit is reached. Without weights, low-statistics data e.g. on polarization variables may be reproduced unsatisfactorily without significant deterioration of the total \mathcal{L}_{tot} . The likelihood function is normalized to avoid an artificial increase in statistics.

Tables 1-5 display the large number of pion- and photo-induced reactions used in the coupled channel analysis presented here. The data comprise nearly all important reactions

including multiparticle final states. Resonances with sizable coupling constants to πN and γN are thus unlikely to escape the fits even though further single and double polarization experiments are certainly needed to unambiguously constrain the contributing amplitudes.

2.2 Recent partial wave analyses

At the time when new photo-production experiments came into sight promising precise data on differential cross section and on asymmetries due to photon-, target- and/or recoil-polarization, several groups enforced their efforts to re-fit older data on pion- and photo-induced reactions, and new groups were formed. The aim was to be prepared for an analysis of the forthcoming data, to fit the data, to extract properties of baryon resonances and to give interpretations of the spectrum of resonances and of the reaction dynamics. This is not a review, hence we just quote from major groups a few recent papers or a review where references to earlier work can be found.

From the three “classical” analysis groups [1,2,3], only the GWU group is still active in methodology [121] and data analysis [122]. Some of their recent results can be found in [123, 124, 125, 126, 127]. We mention here the work of Bennhold and Haberzettl and collaborators [128, 129, 130], also working at GWU. The physics at MAMI (among other data) has been closely followed by the MAID group of Drechsel and Tiator [131, 132, 133, 134, 135, 136, 137, 138]. Smaller groups at Zagreb [139, 140, 141, 142], Gent [143, 144, 145, 146] and KVI made significant contributions to the field [147, 148, 149, 150, 151]. A few further papers are to be mentioned [152, 153, 154, 155, 156].

Strong groups have been formed at Jlab and Bonn/Jülich. At Jlab, the EXCITED BARYON ANALYSIS CENTER [157] was formed with the ambitious goal to extract and interpret properties of nucleon resonances from the world data of meson production reactions induced by pions, photons and electrons. In a dynamical coupled-channel model, πN elastic scattering [158], photoproduction of pions [159], the reaction $\pi^- p \rightarrow n\eta$ [160], and pion and photo-induced production of hyperons [161] are analyzed and properties of contributing resonances are determined. The Bonn/Jülich group has over the years developed a unitary coupled channel exchange model that obeys the strictures from analyticity [162, 163, 164, 165]. For kaon photo- and electroproduction off protons, a gauge invariant chiral unitarity framework was developed in [166]. Also considered are Regge models [167, 168, 169, 170] and heavy mesons [171]. The Gießen group [172, 173, 174, 175, 176, 177, 178, 179, 180, 181] pioneered coupled-channel analyses of large data sets.

2.3 The PWA method

The approach used for the construction of amplitudes for pion and photo-induced reactions is described in [182, 183]. A shorter survey can be found in [8]. Here, we give explicit formulas for differential cross section and recoil polarization for pion-induced production of a spin-1/2 baryon and a pseudoscalar meson.

For πN transition into the channels πN , ηN , $K\Lambda$ and $K\Sigma$, the amplitude can be written as

$$\begin{aligned} A_{\pi N} &= \omega^* [G(s, t) + H(s, t)i(\sigma\mathbf{n})] \omega' , \\ G(s, t) &= \sum_L [(L+1)F_L^+(s) + LF_L^-(s)] P_L(z) , \\ H(s, t) &= \sum_L [F_L^+(s) - F_L^-(s)] P_L'(z) . \end{aligned} \quad (4)$$

with $z = \cos \Theta$, Θ the scattering angle of the outgoing meson in the center-of-mass system (cms), and the decay plane normal

$$\mathbf{n}_j = \varepsilon_{\mu\nu j} \frac{q_\mu k_\nu}{|\mathbf{k}||\mathbf{q}|} . \quad (5)$$

The amplitudes $F_L^\pm(s)$ are related to the scattering amplitude $T_L^\pm(s)$ known from S -matrix theory by

$$T_L^\pm(s) = \frac{2q}{\sqrt{s}} F_L^\pm(s) \quad (6)$$

Here, \mathbf{q} is the initial cms momentum, q its modulus, \mathbf{k} is the final cms momentum. ω and ω' are the spinors of the nucleons in the initial and the final state, and $\varepsilon_{\mu\nu j}$ is the antisymmetric tensor. The functions F_L^\pm depend only on the invariant mass squared s , the ‘+’ functions describe the $1/2^-, 3/2^+, 5/2^-, \dots$ states and ‘-’ functions describe $1/2^+, 3/2^-, 5/2^+, \dots$ states. P_L are Legendre polynomials in z and P_L' are their derivatives.

At fixed energy the unpolarized cross section is proportional to the amplitude squared

$$|A|^2 = \frac{1}{2} \text{Tr} [A_{\pi N}^* A_{\pi N}] = |G(s, t)|^2 + |H(s, t)|^2 (1 - z^2) \quad (7)$$

and the recoil asymmetry can be calculated as:

$$P = \frac{\text{Tr} [A_{\pi N}^* \sigma_2 A_{\pi N}]}{2|A|^2 \cos \phi} = \sin \Theta \frac{2\text{Im}(H^*(s, t)G(s, t))}{|A|^2} . \quad (8)$$

Near threshold, only contributions from S and P -waves are expected. For the $S_{2I,2J}$ and $P_{2I,2J}$ amplitudes we have

$$\underline{S_{2I,1}}; \quad G = F_0^+; \quad H = 0; \quad |A|^2 = |F_0^+|^2 \quad (9a)$$

$$\underline{P_{2I,1}}; \quad G = F_1^- z; \quad H = -F_1^-; \quad |A|^2 = |F_1^-|^2 \quad (9b)$$

$$\underline{P_{2I,3}}; \quad G = 2F_1^+ z; \quad H = F_1^+; \quad |A|^2 = |F_1^+|^2 (3z^2 + 1) \quad (9c)$$

where the indices $(2I, 2J)$ remind of the isospin I and the spin J of the partial waves.

The recoil asymmetry vanishes unless different amplitudes interfere. Thus,

$$\begin{aligned} \underline{S_{2I,1} + P_{2I,1}} : \quad & P \frac{|A|^2}{\sin \Theta} = -2\text{Im}(F_0^+ F_1^{-*}) \quad (10a) \\ |A|^2 = & |F_0^+|^2 + |F_1^-|^2 + 2z\text{Re}(F_0^+ F_1^{-*}) \end{aligned}$$

$$\begin{aligned} \underline{S_{2I,1} + P_{2I,3}} : \quad & P \frac{|A|^2}{\sin \Theta} = 2\text{Im}(F_0^+ F_1^{+*}) \quad (10b) \\ |A|^2 = & |F_0^+|^2 + |F_1^+|^2 (3z^2 + 1) + 4z\text{Re}(F_0^+ F_1^{+*}) \end{aligned}$$

$$\begin{aligned} \underline{P_{2I,1} + P_{2I,3}} : \quad & P \frac{|A|^2}{\sin \Theta} = 6z\text{Im}(F_1^{+*} F_1^-) \quad (10c) \\ |A|^2 = & |F_1^+ - F_1^-|^2 + z^2 (3|F_1^+|^2 - 2\text{Re}(F_1^{+*} F_1^-)) . \end{aligned}$$

where $|A|^2$ represents the angular distribution and $P|A|^2/\sin\Theta$ an observable proportional to the recoil polarization parameter P .

The interference of $1/2^-$ and $1/2^+$ waves leads to a dependence of the differential cross section linear in z while the recoil asymmetry multiplied by the differential cross section and divided by $\sin\Theta$ should be flat. The interference of $1/2^-$ and $3/2^+$ also produces a flat distribution for $P|A_n|^2/\sin\Theta$ while the differential cross section has a z^2 term. The interference between the $1/2^+$ and $3/2^+$ waves provides a symmetric differential cross section and a $P|A_n|^2/\sin\Theta$ distribution proportional to z .

The F_{37} wave is one of the dominant waves in the $\pi^+p \rightarrow K^+\Sigma^+$ reaction. Its amplitude can be cast into the form

$$F_{2I,7} \quad G = 2(5z^3 - z)F_3^+ \quad H = \frac{F_3^+}{2}(15z^2 - 3) \quad (11)$$

and the amplitude squared:

$$|A|^2 = |F_3^+|^2 \frac{1}{4} (175z^6 - 165z^4 + 45z^2 + 9). \quad (12)$$

Its interference with one of the S - or P -waves, written in the form $P \frac{|A_n|^2}{\sin\Theta}$, is calculated to

$$S_{2I1} + F_{2I7} : \quad P \frac{|A|^2}{\sin\Theta} = 3(5z^2 - 1) \text{Im}(F_0^+ F_3^{+*}) \quad (13a)$$

$$P_{2I,1} + F_{2I,7} : \quad P \frac{|A|^2}{\sin\Theta} = 5(7z^3 - 3z) \text{Im}(F_1^- F_3^{+*}) \quad (13b)$$

$$P_{2I,3} + F_{2I,7} : \quad P \frac{|A|^2}{\sin\Theta} = 2(5z^3 + 3z) \text{Im}(F_1^+ F_3^{+*}) \quad (13c)$$

2.4 Features of the data in the threshold region

2.4.1 The reaction $\pi^-p \rightarrow K^0\Lambda$

In a first attempt we try to identify evolving features of the data without or with minimal use of the partial wave analysis. The differential cross section for the reaction $\pi^-p \rightarrow K^0\Lambda$ is shown in Fig. 1. We mention that resonances which may be observed in this reaction belong to the nucleon excitation series; Δ resonances do not couple to ΛK . The observable $Pd\sigma/(d\Omega \sin\Theta)$ in the region near threshold is shown in Fig. 2. To construct this observable the differential cross section was taken from the result of the fit shown as curves in Fig. 1. We use the differential cross sections from the fit to avoid additional statistical fluctuations. Of course, a numerical summation of the differential cross sections would result in very similar distributions. Hence the distributions in Fig. 2 can be considered as purely experimental ones. Several observations can be made:

1. From the threshold region up to ≈ 1750 MeV, the angular distribution ($d\sigma/d\Omega$) rises nearly linearly in $\cos\Theta$ due to the interference of S_{11} and P_{11} waves (see eq. 10a).
2. There is a small quadratic part, indicating contributions from the P_{13} wave (eq. 9c) or from the interference of S_{11} and/or P_{11} with the P_{13} wave (eqs. 10b, 10c).

3. Above 1850 MeV the angular distribution has a strong $1 + 3\cos^2\Theta$ contribution signaling a large P_{13} wave (eq. 9c), and a linear part due to interference with the S_{11} wave (eq. 10b).
4. Near threshold, the $Pd\sigma/(d\Omega \sin\Theta)$ observable is non-zero, almost flat, and shows a small linear rise. The flat part indicates interference between S and P -waves (eqs. 10a, 10b), the linear rise interference between the P_{11} and P_{13} waves (eq. 10c). The linear part becomes more significant in the 1650-1725 MeV region.
5. In the region from 1800 to 2000 MeV, the $Pd\sigma/(d\Omega \sin\Theta)$ polarization has a more complicated angular dependence which indicates the presence of higher waves.
6. The form of the angular distribution and of $Pd\sigma/(d\Omega \sin\Theta)$ change rapidly with energy suggesting that resonances play an important role in the dynamics.

These qualitative results are confirmed in the quantitative partial wave analysis which will be discussed below. Here we just emphasize, in Figs. 1-3, that the data are well reproduced by our fits. The description of the rotation parameter β mea-

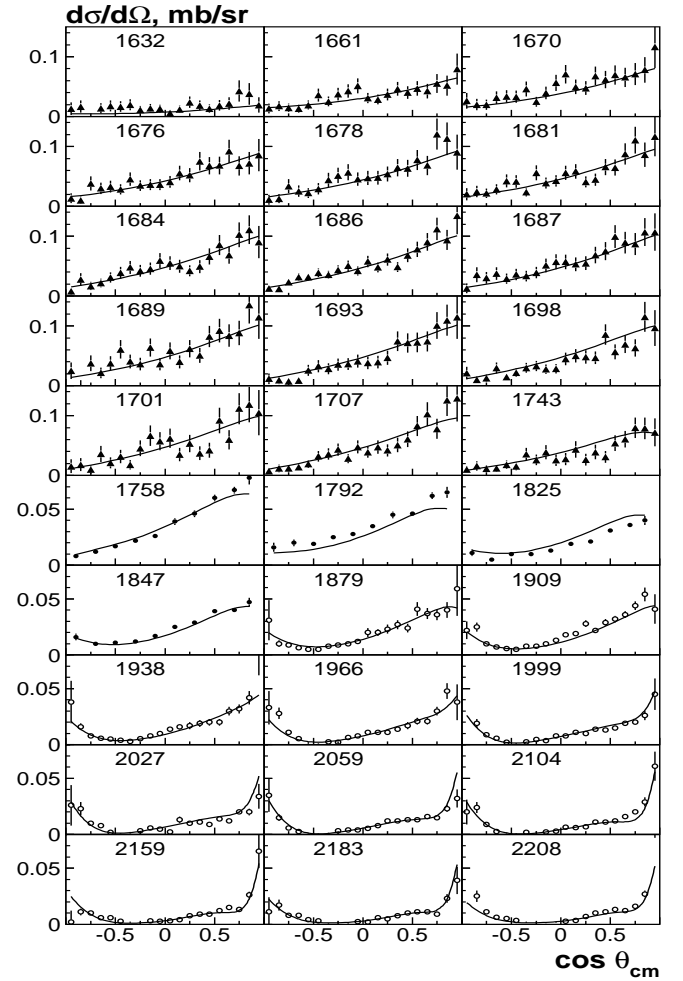


Fig. 1. The differential cross section for the reaction $\pi^-p \rightarrow K^0\Lambda$. The triangles denote the data from [20] and open circles the data from [21, 22], the curves represent our fit BG2010-02.

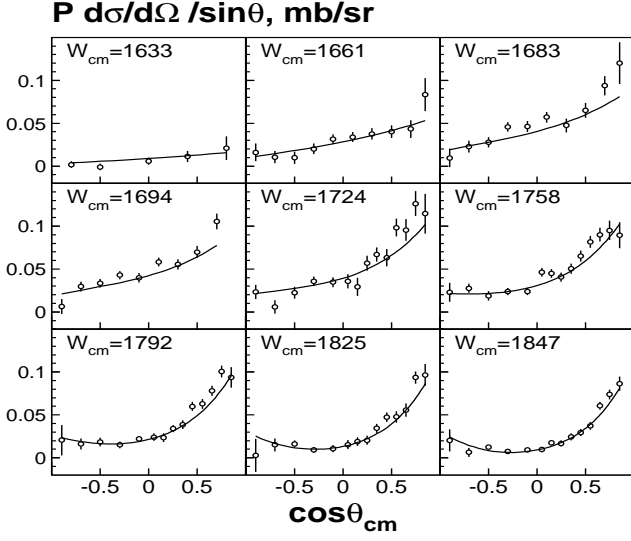


Fig. 2. The $Pd\sigma/(d\Omega \sin \Theta)$ observable for the reaction $\pi^-p \rightarrow K^0\Lambda$. The recoil asymmetry data are from [21,22], the curves represent our fit BG2010-02.

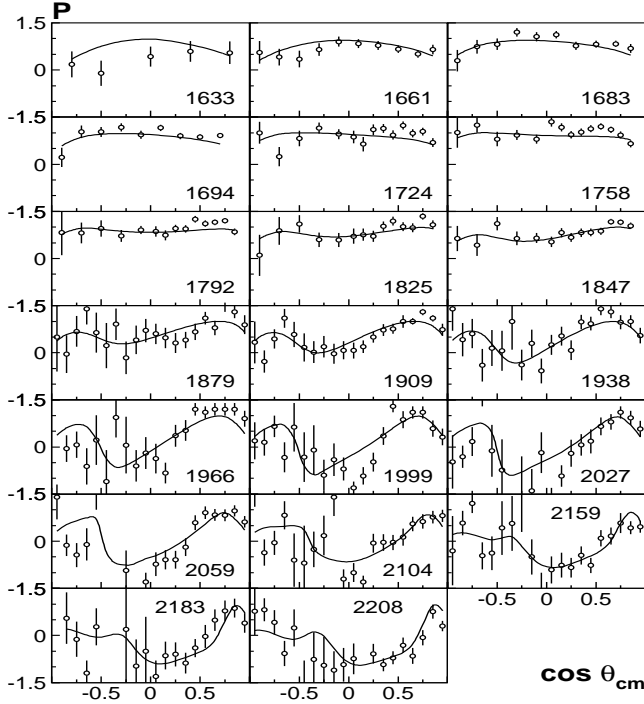


Fig. 3. The recoil asymmetry for $\pi^-p \rightarrow K^0\Lambda$. The open circles denote the data from [21,22], the curves represent our fit BG2010-02.

sured in the experiment [23] is shown in Fig. 4. There are some systematic deviations in the very forward region. However, there might be a problem with these data points or/and with the given errors. The observable A can be written as

$$A = (1 - P^2)^{\frac{1}{2}} \cos \beta = \frac{|G|^2 - |H|^2(1 - z^2)}{|G|^2 + |H|^2(1 - z^2)}. \quad (14)$$

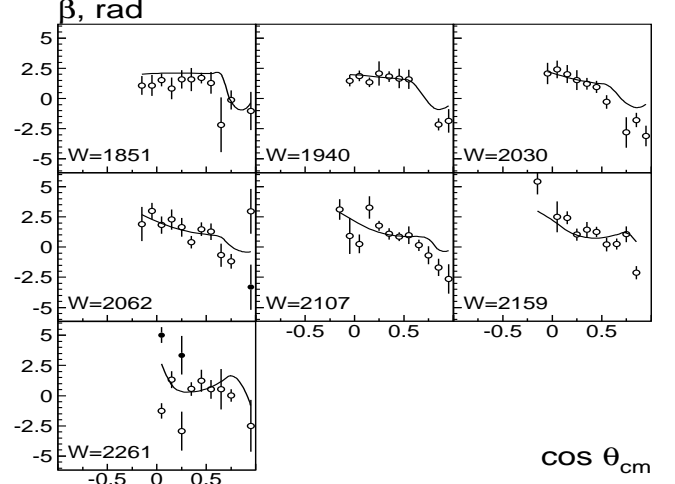


Fig. 4. The rotation parameter for $\pi^-p \rightarrow K^0\Lambda$. The open circles denote the data from [23], the full circles show the mirror points (due to the 2π ambiguity of β), and the curves represent our fit BG2010-02.

At $z = \pm 1$, A must be equal to $+1$ while for the very forward measured points at $\cos \Theta = 0.95$ this observable are close to -1 . We did not find such an extreme oscillatory behavior of this observable.

2.4.2 The reaction $\pi^+p \rightarrow K^+\Sigma^+$

In a next step, we discuss the reaction $\pi^+p \rightarrow K^+\Sigma^+$. In this reaction, all contributing s-channel resonances must belong to the Δ series. Again, we can draw some qualitative conclusions which do not depend on the partial wave analysis.

The differential cross section for $\pi^+p \rightarrow K^+\Sigma^+$ is shown in Fig. 5 and the observable $Pd\sigma/(d\Omega \sin \Theta)$ in the first nine bins is shown in Fig. 6. The best evidence for the existence of $\Delta(1920)P_{33}$ is derived from this reaction.

1. In the threshold region, the angular distribution exhibits two extreme values indicating the presence of a z^3 term, likely due to interference of P_{31} or P_{33} with the F_{37} wave (eqs. 13b, 13c).
2. The recoil polarization below 1900 MeV is comparatively small which points at the dominance of one particular wave.
3. The angular distribution prefers P_{33} (eq. 9c) compared to P_{31} (eq. 9b) as dominant wave.
4. Above 1940 MeV the recoil polarization is large and even approaches the extreme values ± 1 . Hence there should be two dominant waves; other partial wave distributions are likely small.
5. One of the two waves must be the F_{37} wave. In the mass range from 2000 to 2150 MeV, the angular distribution requires $J^P = 7/2^+$ and interference with other waves. The partial wave analysis identifies the second wave as $5/2^+$ wave.
6. The angular distributions and the recoil asymmetry undergo rapid changes. Hence the partial waves must be resonating.

The experimental cross sections, recoil polarization P and rotation parameter β of the Σ^+ hyperon and the curves result-

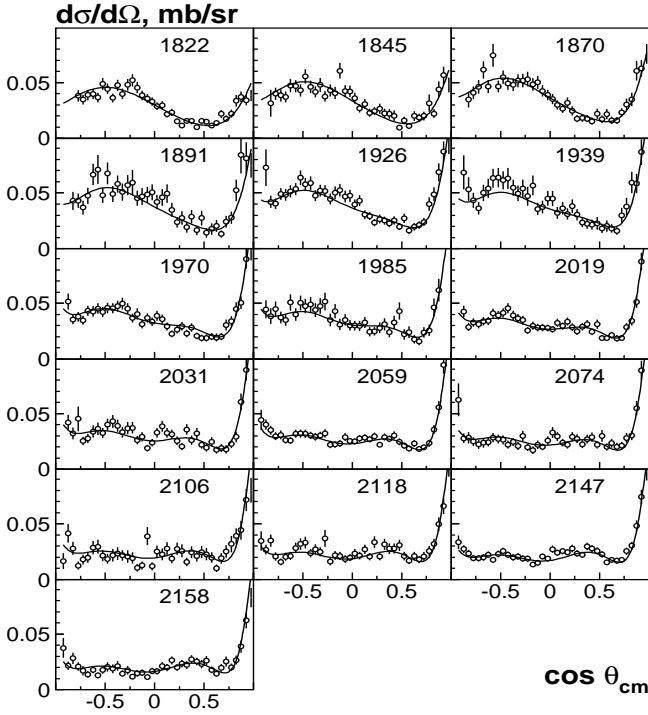


Fig. 5. The differential cross section for the reaction $\pi^+p \rightarrow K^+\Sigma^+$. The data are taken from [24]. The curves represent our fit BG2010-02.

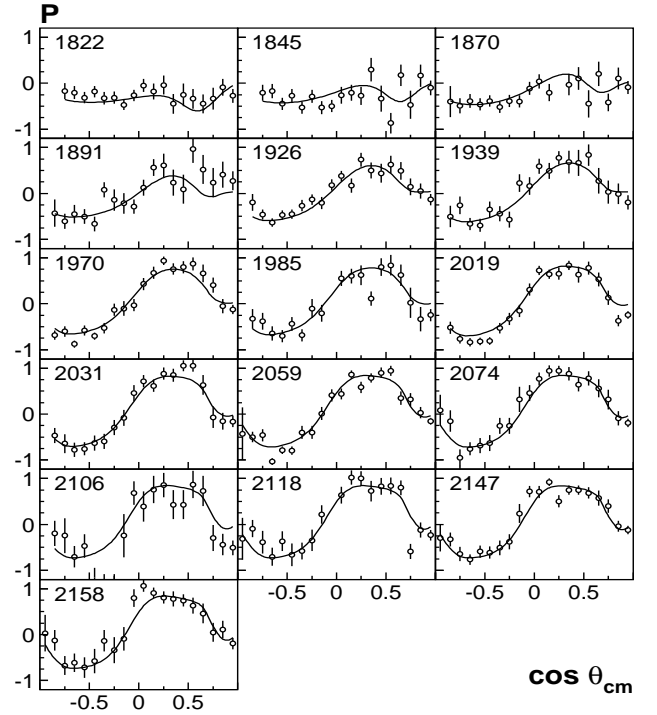


Fig. 7. The recoil asymmetry P for the reaction $\pi^+p \rightarrow K^+\Sigma^+$. The data are from [24], the curves represent our fit BG2010-02.

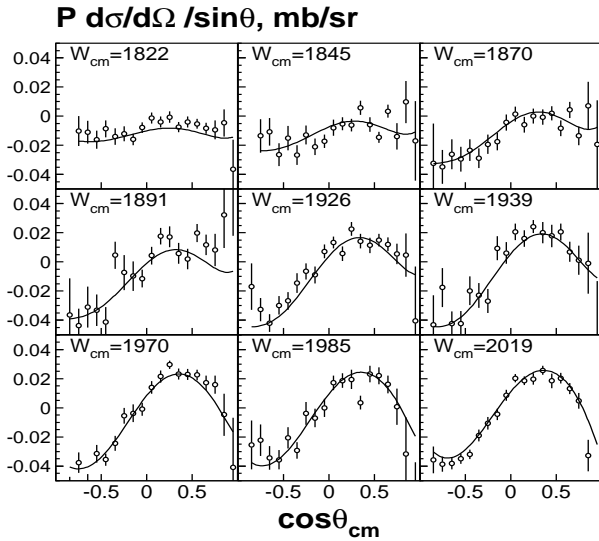


Fig. 6. The $P d\sigma/(d\Omega \sin \Theta)$ observable for the reaction $\pi^+p \rightarrow \Sigma^+K^+$. The data are from [24], the curves represent our fit BG2010-02.

ing from our fits are shown in Fig. 5-8, for the mass region used in the fits.

2.4.3 The reaction $\pi^-p \rightarrow K^0\Sigma^0$

This reaction receives contributions from the nucleon and Δ resonances with masses above 1700 MeV. The contributions of Δ resonances to $\pi^+p \rightarrow K^+\Sigma^+$ and $\pi^-p \rightarrow K^0\Sigma^0$ are

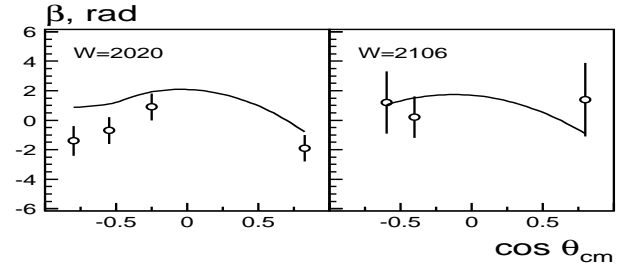


Fig. 8. The rotation parameter for $\pi^+p \rightarrow K^+\Sigma^+$. The open circles denote the data from [23] and the curves represent our fit BG2010-02.

constrained by simple Clebsch-Gordan coefficients. Thus these data supply valuable information about nucleon states decaying into $K\Sigma$ channel and provide a consistency check of the partial wave analysis.

The differential cross section for the reaction $\pi^-p \rightarrow K^0\Sigma^0$ is shown in Fig. 9 and the recoil polarization P in Fig. 10. Data on the cross section are available starting from 1879 MeV only. In the region 1879-1940 MeV the differential cross section is very similar to that for the $\pi^+p \rightarrow K^+\Sigma^+$ reaction, thus Δ resonances seem to play the dominant role. Above 1940 MeV, the structure of the differential cross section is rather complicated due to presence of high partial waves, in particular of the F_{37} -wave. Unfortunately there are no good data for the recoil asymmetry for this reaction: the errors are too large to provide stringent constraints for the fit.

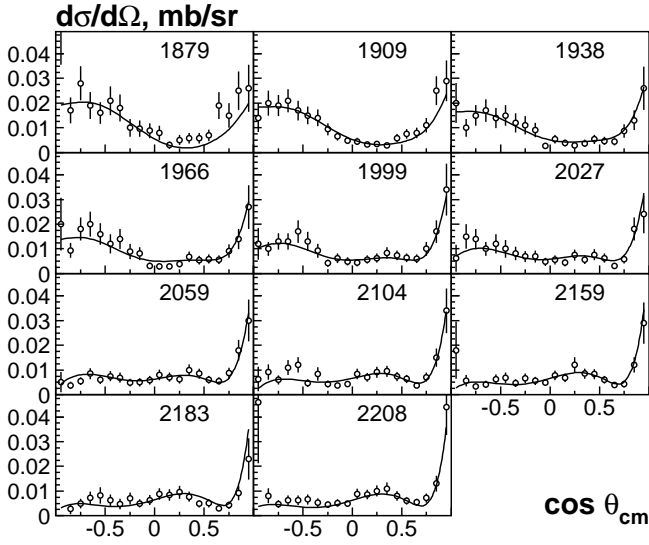


Fig. 9. The differential cross section for the reaction $\pi^-p \rightarrow K^0\Sigma^0$. The open circles denote the data from [26]; the curves represent our fit BG2010-02.

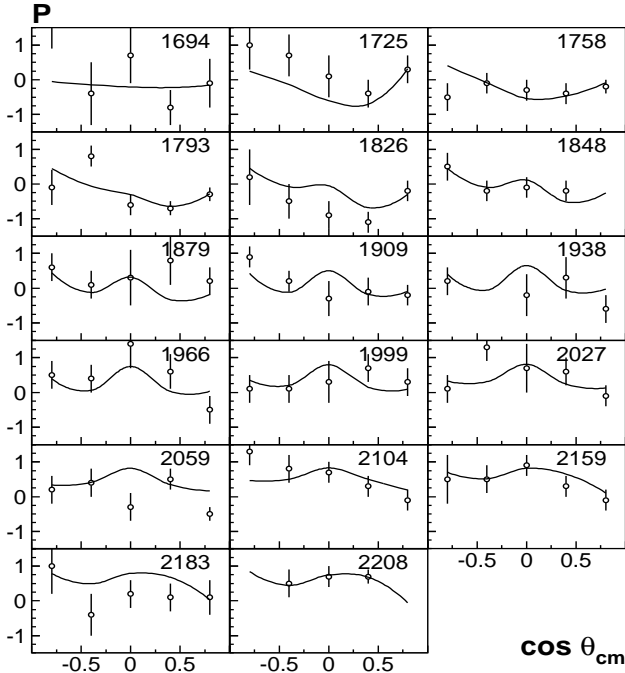


Fig. 10. The recoil asymmetry P for the reaction $\pi^-p \rightarrow K^0\Sigma^0$. The data are taken from [26]; the curves represent our fit BG2010-02.

2.4.4 The reaction $\pi^-p \rightarrow \eta n$

We include a discussion of the reaction $\pi^-p \rightarrow \eta n$, mainly because of negative parity nucleon resonances, even though these will be discussed elsewhere. Differential cross section were reported in [18, 19, 185, 186, 187, 188]; however there are large discrepancies between different data sets at least above 1800 MeV.

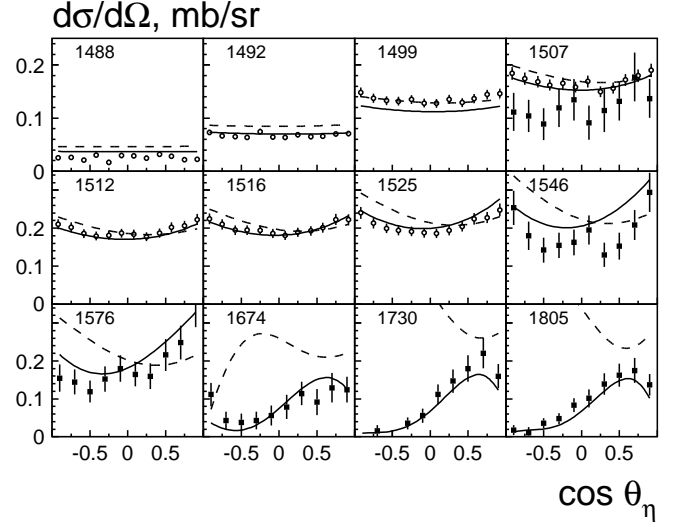


Fig. 11. The differential cross section for the reaction $\pi^-p \rightarrow \eta n$. The open circles denote the data from [19] and full squares the data from [18]. The solid curves represent our fit BG2010-02, the dashed curve an earlier fit [184] which was not constrained by data on $\pi^-p \rightarrow \eta n$.

Here, we fit the precise data from the Crystal Ball collaboration [19]; for the higher energy region, we use the data from [18] since they are mostly compatible with the Crystal Ball data and can probably be trusted up to 1800 MeV. Fig. 11 shows the angular distributions. They are rather flat in the region below 1500 MeV due to dominance of the S_{11} wave. In the region 1600-1800 MeV the angular distribution is very asymmetric, which can come from interference of the S_{11} -wave with either the P_{11} - or P_{13} -wave.

2.5 Leading partial wave contributions

These observations are quantitatively confirmed by the partial wave analysis. In this paper, we focuss on P -wave resonances. Of course, negative-parity resonances and higher partial waves are required as well to fit the data. These will be discussed in detail in a forthcoming publication. In Table 6 we provide a list of states which are included in this analysis but not discussed here. Resonances above 2 GeV are mostly introduced to improve the description in the high-mass region even though we do not claim that they really exist. We also summarize, in Table 7, the background contributions used to describe the pion- and photo-induced data.

The contributions of the dominant waves to the reaction $\pi^-p \rightarrow K^0\Lambda$ are shown in Fig. 12a. At threshold, the dominant wave is S_{11} which decreases fast with increasing energy. Below 1800 MeV, the P_{11} wave is the second strongest wave. It shows a clear resonance behavior peaking at 1720 MeV. The P_{13} wave increases steadily from threshold reaching its maximum at 1900 MeV.

The two largest contributions to the reaction $\pi^+p \rightarrow K^+\Sigma^+$ are assigned to the P_{33} and F_{37} partial waves (see Fig. 12b). When one of the waves is assumed to be non-resonant, angular and recoil distributions cannot be reproduced satisfactorily.

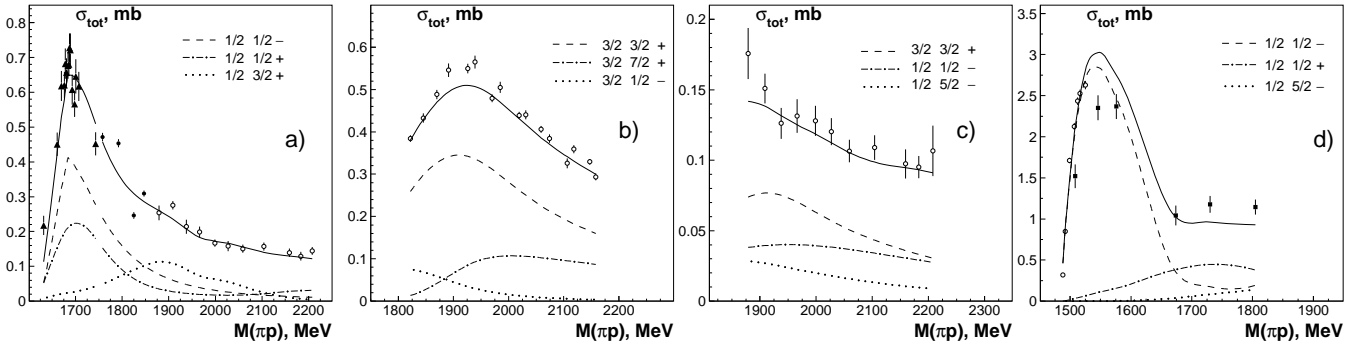


Fig. 12. a) The total cross section for the reaction $\pi^- p \rightarrow K^0 \Lambda$ and contributions from leading partial waves. The full curve shows the integrated fit of the differential cross section from the solution BG2010-02. The full triangles denote the total cross section calculated from [20] and the open circles from [21],[22]. b) The total cross section for the reaction $\pi^+ p \rightarrow K^+ \Sigma^+$ and contributions from leading partial waves. The full curve shows the integrated fit of the differential cross section from the solution BG2010-02. The data points show the total cross section calculated from [24]. c) The total cross section for the reaction $\pi^- p \rightarrow K^0 \Sigma^0$ and contributions from leading partial waves. d) The total cross section for the reaction $\pi^- p \rightarrow \eta n$ and contributions from leading partial waves.

The energy dependence of the F_{37} wave in this reaction is compatible with the well known $F_{37}(1950)$ state. We found only a rather small (below 1%) contribution from $\Delta(1905)F_{35}$. The P_{33} wave has a maximum in the region 1900 MeV which is expected if the $\Delta(1920)P_{33}$ state provides a large contribution.

The contribution from Δ -states to $\pi^- p \rightarrow K^0 \Sigma^0$ can be fixed, using the isotopic relations, from a fit of the $\pi^+ p \rightarrow K^+ \Sigma^+$ reaction. These partial waves provide about 70% to the total cross section and contributions from nucleon partial waves are needed to describe the remaining part of the data. In the 1850-1950 MeV region one of the largest contributions is due to the D_{13} wave, which decreases fast with energy. This indicates the presence of a resonance with a mass just below the energy region covered by the data. The total cross section and contributions from leading partial waves are shown in Fig. 12c.

The total cross section for $\pi^- p \rightarrow \eta n$ calculated from the fitted differential cross section is shown in Fig. 12d. At low

energies the cross section is dominated by the $N(1535)S_{11}$ contribution. The $N(1650)S_{11}$ resonance does not provide any visible structure to the S_{11} partial wave. In the 1700-1900 MeV region, the P -wave amplitudes describe about 50% of the total cross section. However the lack of polarization information does not allow us to determine them uniquely. There are two sets of solutions (with BG2010-01 and BG2010-02 as best solutions) which lead to rather different amplitudes for the P_{11} and P_{13} partial waves (Fig. 13) and to different P_{11} pole positions (see Table 9 below). In any case, these data impose important limits on the ηN couplings of the P -wave states.

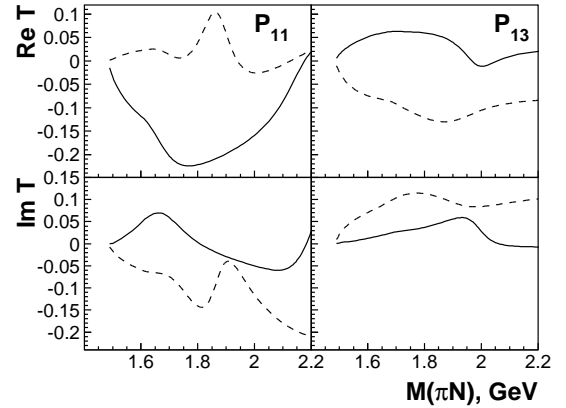


Fig. 13. The $\pi^- p \rightarrow \eta n$ transition amplitude in the P_{11} and P_{13} wave. The full curve corresponds to the solution BG2010-02, the dashed curve to BG2010-01.

Table 6. List of the S , D , F , and G -wave resonances used in the combined analysis of the data. Known states are listed by the PDG names. Resonances with a J^P subscript are not listed in [7].

$N(1535)S_{11}$	$N(1650)S_{11}$	$N_{1/2-}(1890)$	$N(1520)D_{13}$
$N(1700)D_{13}$	$N_{3/2-}(1875)$	$N_{3/2-}(2130)$	$N(1675)D_{15}$
$N_{5/2-}(2070)$	$N(1680)F_{15}$	$N(2000)F_{15}$	$N(1990)F_{17}$
$N(2190)G_{17}$	$N(1620)S_{31}$	$\Delta(1900)S_{31}$	$\Delta(1700)D_{33}$
$\Delta(1940)D_{33}$	$\Delta_{3/2-}(2200)$	$\Delta(1905)F_{35}$	$\Delta(1950)F_{37}$

Table 7. Background amplitudes used in the combined analysis of the data.

	pion-induced	photo-induced
t -channel exchange		$\pi^\pm, \rho^0/\omega, \rho^\pm$
	$K^{*0}, K^{*\pm}$	$K^\pm, K^{*0}, K^{*\pm}$
u -channel exchange		$N(938), \Lambda, \Sigma^0, \Sigma^\pm$
	Direct production of final-state particles	

2.6 The new data on the $\gamma p \rightarrow K \Lambda$ reaction

The new CLAS data on the $\gamma p \rightarrow K \Lambda$ reaction [112] cover a wide mass range and exceed in statistics all previously reported measurements of this reaction. Also the angular range

has been extended in comparison with earlier CLAS data. We have therefore decided to use this data set only for the new fits.

The data cover the invariant mass region from the $K\Lambda$ threshold up to 2.8 GeV. In the present analysis, we use these data up to 2.4 GeV; the higher energy region will be subject of future investigations. At low energies the differential cross sections (see Fig. 14) show an almost linear dependence on $\cos\Theta$ which can be explained by the interference of S_{11} and P -wave amplitudes. An already satisfactory fit of a smaller data set was obtained with the set of resonances reported in [8]. Then we added in the fit, one by one, different resonances parameterized as relativistic multi-channel Breit-Wigner amplitudes. We found a significant improvement from a S_{11} state, which optimized at a mass of 1886 ± 10 MeV and 80 ± 15 MeV width. It is remarkably close to the result obtained by Höhler [1]. New double polarization data in this region are urgently needed to provide a final proof for the existence of this state.

We found a notable improvement from two other states: from $N(1990)F_{17}$ and $N(2190)G_{17}$, both with masses compatible with PDG values [7]. Both states also help to achieve a good description of the new CLAS data. A full report about properties of the S_{11} partial wave and the investigation of the F_{17} and G_{17} states will be given elsewhere.

The final description of the recoil asymmetry is shown in Fig. 15. There are significant problems in the low-energy region. These are rather local and would require introduction of new and narrow resonances. We refrain to do so before more convincing experimental evidence exists. Systematic deviations show up in the backward region in the 2120-2250 MeV invariant mass interval. However, we did not find a single resonance which would improve notably the description. It is quite possible that the data indicate the presence of a few new states with different quantum numbers in this region but from the analysis of the present data set, no firm conclusions can be drawn.

The contribution of S and P -waves to the total cross section is shown in Fig. 16. As before the full curve is calculated by integration of our fitted differential cross sections over the full angular range; the data points are determined from a summation of the measured differential cross sections over the angular range where data exist, the uncovered angular range is taken into account by adding the fit values for the differential cross sections.

The S_{11} and P_{13} partial waves have a similar strength and both show evidence for two peaks; both partial waves exhibit a threshold effect and rise steeply at threshold. The threshold peaks indicate the presence of resonances close to 1700 MeV. The S_{11} partial wave shows a second peak just below 1900 MeV, the P_{13} partial wave at about 1940 MeV. The P_{11} partial wave is smoother and shows a peak in the 1780 MeV region and possibly a broad shoulder with a possibility of a second structure at or above 1900 MeV.

3 Discussion of partial waves

In this section, we discuss the individual partial waves, P_{33} , P_{31} , P_{13} , and P_{11} , and their resonant contributions. The pole positions of the transition amplitudes between channels $i, j =$

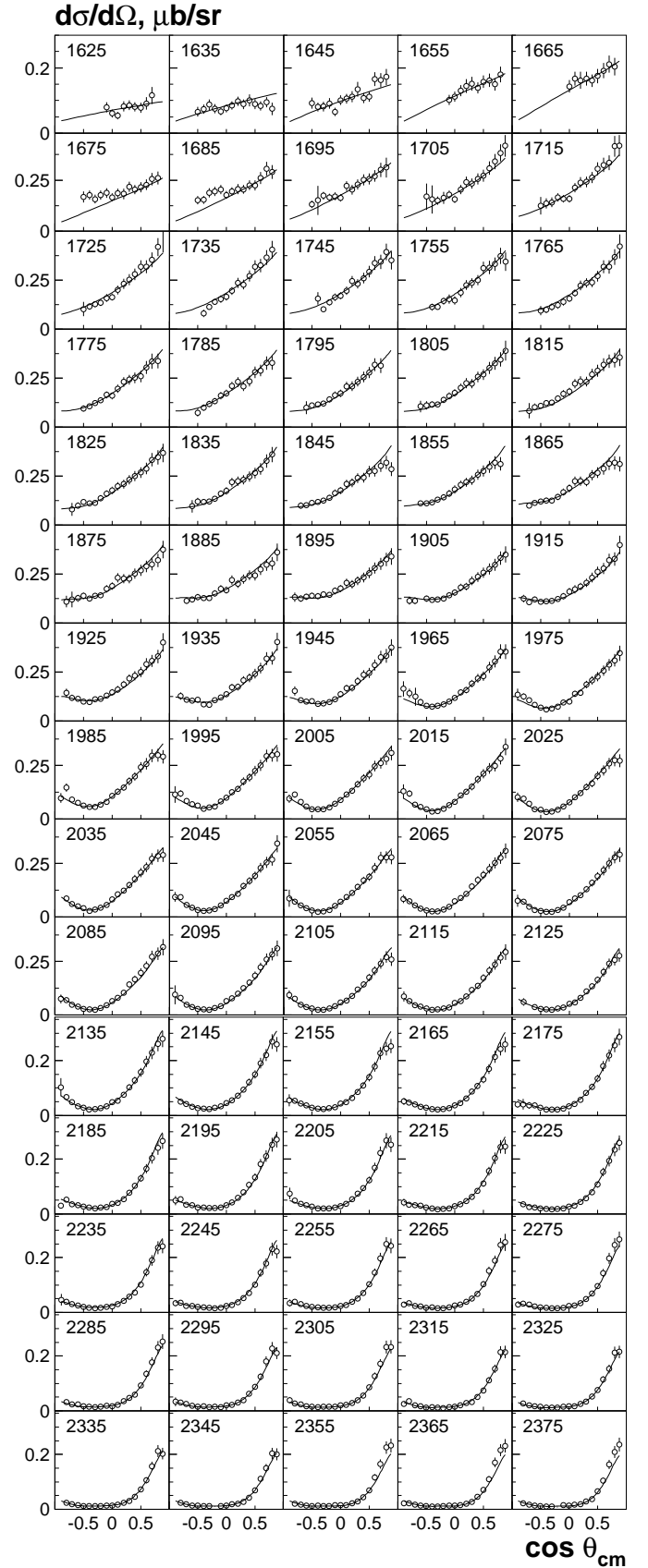


Fig. 14. Differential cross section for $\gamma p \rightarrow K\Lambda$. The data are from [112]. The full curve corresponds to the solution BG2010-02.

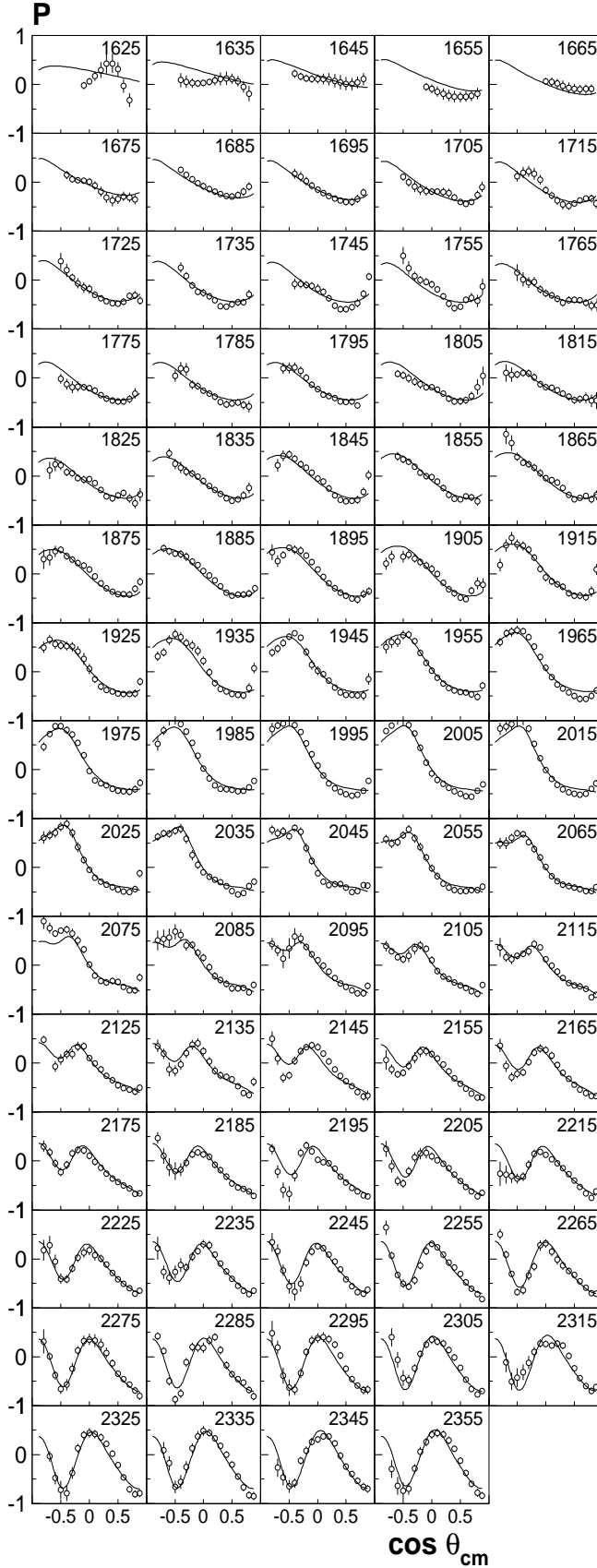


Fig. 15. The $\gamma p \rightarrow K\Lambda$ recoil asymmetry. The data are from [112]. The full curve corresponds to the solution BG2010-02.

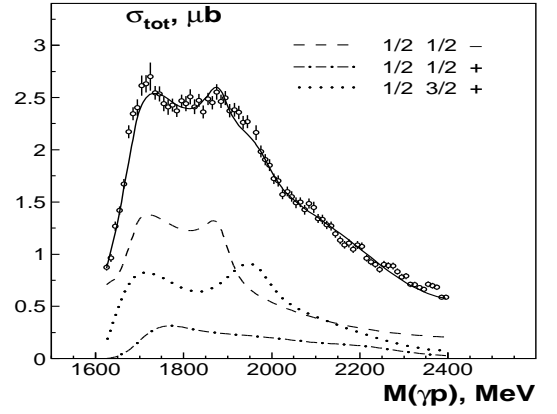


Fig. 16. Contributions from the S and P -wave to $\gamma p \rightarrow K\Lambda$. The full curve shows the integrated fit of the differential cross section from the solution BG2010-02. The open circles denote the total cross section calculated from [112].

Table 8. Pole positions and residues of the transition amplitudes (given in MeV as $|r|/\Theta$ with $ResA = |r|e^{i\Theta}$). The phases are given in degrees. The helicity couplings are given in $GeV^{-1/2}$. The errors are defined from the spread of results found in the respective classes of solutions. The PDG values are given in parentheses.

State	$\Delta(1232)P_{33}$	$N(1440)P_{11}$
Re(pole)	1210 ± 1 (1210 ± 1)	1377 ± 6 (1365 ± 15)
$-2\text{Im}(\text{pole})$	100 ± 1 (100 ± 2)	190 ± 12 (190 ± 30)
$A(\pi N \rightarrow \pi N)$	$51.4 \pm 0.5 / -47 \pm 1^\circ$	$47 \pm 3 / -83 \pm 10^\circ$
$A(\pi N \rightarrow \eta N)$		$5 \pm 3 / 160 \pm 60^\circ$
$A^{1/2}(\gamma p)$	$132.5 \pm 2 / 165 \pm 2^\circ$	$-40 \pm 10 / -37 \pm 10^\circ$
$A^{3/2}(\gamma p)$	$261 \pm 2 / 178 \pm 2^\circ$	
State	$N(1900)P_{13}$	$N_{3/2+}(1975)$
Re(pole)	1890 ± 50 (~ 1900)	1970 ± 25 (-)
$-2\text{Im}(\text{pole})$	270^{+180}_{-100} (-)	250 ± 60 (-)
$A(\pi N \rightarrow \pi N)$	$3 \pm 2 / -20 \pm 40^\circ$	$2 \pm 1 / 80 \pm 40^\circ$
$A(\pi N \rightarrow \eta N)$	$6 \pm 3 / 80 \pm 40^\circ$	$4 \pm 2.5 / 10 \pm 60^\circ$
$A(\pi N \rightarrow K\Lambda)$	$14 \pm 6 / 145 \pm 25^\circ$	$5 \pm 3 / -10 \pm 40^\circ$
$A(\pi N \rightarrow K\Sigma)$	$6 \pm 4 / 80 \pm 50^\circ$	$1.5 \pm 0.5 / -30 \pm 50^\circ$
$A^{1/2}(\gamma p)$	$70 \pm 25 / 130 \pm 40^\circ$	$-8 \pm 8 / -20 \pm 50^\circ$
$A^{3/2}(\gamma p)$	$110 \pm 60 / 170 \pm 35^\circ$	$50 \pm 30 / 25 \pm 45^\circ$
State	$\Delta(1910)P_{31}$	$\Delta(1920)P_{33}$
Re(pole)	1900 ± 40 (1900 ± 50)	1930 ± 40 (1900 ± 50)
$-2\text{Im}(\text{pole})$	500^{+50}_{-100} (300 ± 100)	300 ± 50 (300 ± 100)
$A(\pi N \rightarrow \pi N)$	$38 \pm 8 / -125 \pm 15^\circ$	$10 \pm 6 / 20 \pm 60^\circ$
$A(\pi N \rightarrow K\Sigma)$	$19 \pm 4 / -80 \pm 20^\circ$	$10 \pm 5 / 150 \pm 30^\circ$
$A^{1/2}(\gamma p)$	$55 \pm 20 / 80 \pm 70^\circ$	$120 \pm 35 / -120 \pm 35^\circ$
$A^{3/2}(\gamma p)$		$110 \pm 30 / -170 \pm 30^\circ$

πN , ηN , $K\Lambda$, $K\Sigma \dots$

$$T_L^\pm(i \rightarrow j) = \sqrt{\rho_i} \sum_a K_{ia}^{\pm L} (I - i\rho K^{\pm L})_{aj}^{-1} \sqrt{\rho_j} \quad (15)$$

are calculated as residues in the energy complex plane and given in Tables 8 and 9. Note that our helicity couplings $A_{1/2}$ and $A_{3/2}$ are defined at the pole position and are complex num-

Table 9. Pole positions and residues of the transition amplitudes (given in MeV as $|r|/\Theta$ with $ResA = |r|e^{i\Theta}$). The phases are given in degrees. The helicity couplings are given in $GeV^{-1/2}$. The errors are defined from the spread of results found in both classes of solutions. The PDG values are given in parentheses.

Solution	01	02
State	$N(1710)P_{11}$	$N(1710)P_{11}$
Re(pole)	1690^{+25}_{-10} (1720±50)	1695 ± 15 (1720±50)
-2Im(pole)	210 ± 25 (230±150)	220 ± 30 (230±150)
$A(\pi N \rightarrow \pi N)$	$5 \pm 4 / -80 \pm 40^\circ$	$7 \pm 3 / 170 \pm 25^\circ$
$A(\pi N \rightarrow \eta N)$	$8 \pm 4 / 20 \pm 20^\circ$	$6 \pm 4 / 40 \pm 15^\circ$
$A(\pi N \rightarrow K\Lambda)$	$17 \pm 4 / -110 \pm 20^\circ$	$16 \pm 5 / -110 \pm 15^\circ$
$A(\pi N \rightarrow K\Sigma)$	$3 \pm 2 / 20 \pm 40^\circ$	$5 \pm 3 / 20 \pm 20^\circ$
$A^{1/2}(\gamma p)$	$80 \pm 25 / 100 \pm 30^\circ$	$35 \pm 20 / -35 \pm 20^\circ$
State	$N_{1/2+}(1875)$	$N_{1/2+}(1875)$
Re(pole)	1860 ± 20 ()	1850^{+20}_{-50} ()
-2Im(pole)	110^{+30}_{-10} ()	360 ± 40 ()
$A(\pi N \rightarrow \pi N)$	$2 \pm 2 / 30 \pm 30^\circ$	$15 \pm 7 / 75 \pm 30^\circ$
$A(\pi N \rightarrow \eta N)$	$8 \pm 4 / -40 \pm 30^\circ$	$11 \pm 4 / 0 \pm 20^\circ$
$A(\pi N \rightarrow K\Lambda)$	$0.5 \pm 0.5 / 10 \pm 30^\circ$	$14 \pm 5 / 90 \pm 30^\circ$
$A(\pi N \rightarrow K\Sigma)$	$3 \pm 2 / 160 \pm 25^\circ$	$10 \pm 3 / -120 \pm 20^\circ$
$A^{1/2}(\gamma p)$	$12 \pm 6 / -80 \pm 40^\circ$	$55 \pm 15 / 70 \pm 30^\circ$
State	$N(1720)P_{13}$	$N(1720)P_{13}$
Re(pole)	1695 ± 30 (1675±15)	1670 ± 30 (1675±15)
-2Im(pole)	400 ± 60 (190±85)	420 ± 60 (190±85)
$A(\pi N \rightarrow \pi N)$	$22 \pm 5 / -85 \pm 20^\circ$	$28 \pm 6 / -95 \pm 20^\circ$
$A(\pi N \rightarrow \eta N)$	$9 \pm 4 / -70 \pm 25^\circ$	$8 \pm 3 / -65 \pm 25^\circ$
$A(\pi N \rightarrow K\Lambda)$	$15 \pm 8 / -125 \pm 30^\circ$	$12 \pm 4 / -80 \pm 30^\circ$
$A(\pi N \rightarrow K\Sigma)$	$10 \pm 6 / -80 \pm 25^\circ$	$10 \pm 4 / -30 \pm 40^\circ$
$A^{1/2}(\gamma p)$	$110 \pm 40 / 20 \pm 40^\circ$	$95 \pm 30 / 0 \pm 30^\circ$
$A^{3/2}(\gamma p)$	$130 \pm 50 / 70 \pm 40^\circ$	$115 \pm 30 / 70 \pm 25^\circ$
State	$\Delta(1600)P_{33}$	$\Delta(1600)P_{33}$
Re(pole)	1480 ± 30 (1600±100)	1480 ± 30 (1600±100)
-2Im(pole)	240 ± 40 (300±100)	230 ± 40 (300±100)
$A(\pi N \rightarrow \pi N)$	$14 \pm 3 / -170 \pm 15^\circ$	$14 \pm 3 / -170 \pm 15^\circ$
$A(\pi N \rightarrow K\Sigma)$	$2 \pm 1 / -80 \pm 20^\circ$	$3 \pm 1 / -110 \pm 20^\circ$
$A^{1/2}(\gamma p)$	$26 \pm 6 / -80 \pm 30^\circ$	$16 \pm 5 / 110 \pm 30^\circ$
$A^{3/2}(\gamma p)$	$15 \pm 6 / 0 \pm 20^\circ$	$10 \pm 5 / -150 \pm 30^\circ$

bers. They become real only in the limit of an isolated Breit-Wigner amplitude representation of a resonance.

In spite of the large data base, the partial wave analysis does not converge to a unique solution. Instead, we found two classes of solutions which have rather different imaginary parts for the third P_{11} pole: the first set of solutions has a pole at $1860 \pm 20 - i55^{+15}_{-5}$ MeV (the best solution from this class is called BG2010-01) and second set has a pole at $1850^{+20}_{-50} - i180 \pm 20$ (best solution: BG2010-02). The second solution is well compatible with the result reported in [189]. Within the two classes of solutions, there is a large number of sub-solutions which depend on the model details: the number of poles in the P_{13} wave has an impact on all fit values. For most resonances, the two classes of solutions give compatible re-

sults. Masses, widths, residues and their respective errors for states which are similar in BG2010-01 and BG2010-02 are listed in Table 8, the states which have different properties are listed in Table 9. The spread of results in both sets of solutions is used to estimate the errors.

3.1 $(I)J^P = (3/2)3/2^+$

This wave is, of course, dominated by the well-known $\Delta(1232)$ isobar. This leading resonance is well below the threshold for strangeness production but since the elastic πN scattering and single pion photoproduction data are included in this analysis, the fit returns pole position and Breit-Wigner parameters for this resonance as well. Hence the $\Delta(1232)$ parameters are included in Table 8.

As discussed in the Introduction, the mass region above the $\Delta(1232)$ isobar is controversial. Two further resonances, $\Delta(1600)P_{33}$ and $\Delta(1920)P_{33}$, are seen in the analyses [1, 2, 6] and in inelastic reactions [6, 176, 13] while in [3] – which relies on the most extensive set of data on πN elastic scattering – $\Delta(1600)P_{33}$ is observed as broad structure and $\Delta(1920)P_{33}$ is missing.

We have already reported evidence for the $\Delta(1920)P_{33}$ resonance by a study of the reaction $\gamma p \rightarrow \pi^0 \eta p$ [13]. In a coupled-channel analysis of a large set of data [8], the mass of this state was found to be 1950 ± 40 MeV. The present analysis defines the pole position around 1925 MeV, a compromise between the fit to $\gamma p \rightarrow \pi^0 \eta p$ and the fit to $\pi^+ p \rightarrow K^+ \Sigma^+$ data. In the 3-pole 6-channel K-matrix fit we find the pole at $1925 \pm 40 - i150 \pm 25$. The pole position and residues for the elastic and transition amplitudes are given in Table 8. If the two P_{33} resonances are excluded from the fit, the differential cross section for this reaction shows systematic deviations. A selection of data in comparison to fit results is shown in Fig. 17. When one resonance is removed, the fit decides in favor of $\Delta(1920)P_{33}$ (replacing $\Delta(1600)P_{33}$ by background terms). The total χ^2 deteriorates significantly even though the effect in Fig. 17 is less visible.

Nevertheless, the $\Delta(1600)P_{33}$ state plays an important role for the description of all fitted data, too. The pole position was found to be $1480 \pm 30 - i120 \pm 20$ MeV. If this state is excluded, systematic discrepancies are observed in the description of the P_{33} elastic amplitude (see Fig. 17c). Imposing a very large weight on the elastic data we can reproduce the elastic amplitude also without $\Delta(1600)P_{33}$. Without $\Delta(1600)P_{33}$, the pole representing $\Delta(1920)P_{33}$ moves to a higher mass and becomes broader. However, this fit fails to reproduce accurately the $\pi^+ p \rightarrow K^+ \Sigma^+$ data. This is an example for the main point of this analysis: the elastic amplitude may yield a satisfactory solution (in terms of χ^2) without introduction of a resonance but the inclusion of inelastic reactions may reveal that resonant contributions are required.

To check the stability of the solution we also introduced a further higher-mass P_{33} state, first as a Breit-Wigner resonance and then as forth K-matrix pole. Both parameterizations optimized with a pole at about 2150 MeV mass and 500 MeV width. However, only a marginal improvement was observed in the description of the data.

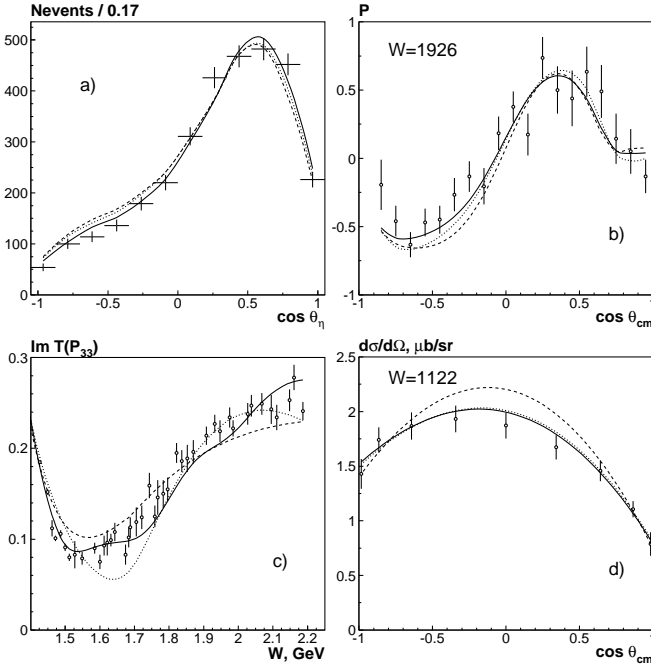


Fig. 17. a) Angular distribution of the η meson for the reaction $\gamma p \rightarrow \pi \eta p$, b) the recoil asymmetry for the reaction $\pi^+ p \rightarrow K^+ \Sigma^+$, c) imaginary part of the πN elastic amplitude and d) $\gamma p \rightarrow \pi^0 p$ differential cross section at low energies. The full curve corresponds to the solution BG2010-02 with two P_{33} states above $\Delta(1232)$, the dotted curve to a solution one state, the dashed curve to a solution with both these states removed from the fit. The data shown contribute only a small fraction of the total χ^2 improvement (Table 10). For the three hypotheses, solution BG2010-02 yields, respectively: a) $\chi^2 = 19, 34, 46$ for 12 data points, b) $\chi^2 = 22.5, 29, 42$ for 19 data points, c) 113, 358, 448 for 40 data points, and d) 4.0, 4.6, 21.2 for 9 data points.

The three pole structure, observed in the P_{33} wave below 2 GeV is not in conflict with the SAID energy-independent partial wave amplitude. The comparison of our curve and the result of the SAID energy-independent phase shift analysis is shown in Fig. 18.

The Höhler solution for the P_{33} wave shows a clear structure in the mass region 1600-2000 MeV which is compatible with our finding. We have added for the fits to real- and imaginary part of the amplitude 2% errors below 1500 MeV and 5% errors above. The result of the fit is shown in Fig. 19. Note that curves in Figs. 18 and 19 represent different fits. However, when the SAID amplitude for the P_{33} -wave is substituted by the Höhler amplitude, only the elastic P_{33} amplitude changes significantly but other results change very little.

The likelihood is not a direct criterium for the fit quality. More interesting are the changes in likelihood when resonances are removed from the fit and the data refitted. In Table 10 we give, for convenience, changes $\Delta\chi^2 = -2\Delta(L_{\text{tot}})$. Solution BG2010-01 is slightly worse than solution BG2010-02, $\Delta\chi^2 = 152$.

Table 10. Changes in χ^2 for solution BG2010-02 when resonances are removed and the data refitted.

removed	$\Delta\chi^2$	removed	$\Delta\chi^2$
$\Delta(1600)P_{33}$	2843	$\Delta(1600)P_{33}$ and $\Delta(1920)P_{33}$	6420
$N_{1/2^+}(1875)$	2154	$N_{1/2^+}(1875)$ and $N(1710)P_{11}$	4756
$N_{3/2^+}(1975)$	1332	$N(1900)P_{13}$ and $N_{3/2^+}(1975)$	3187

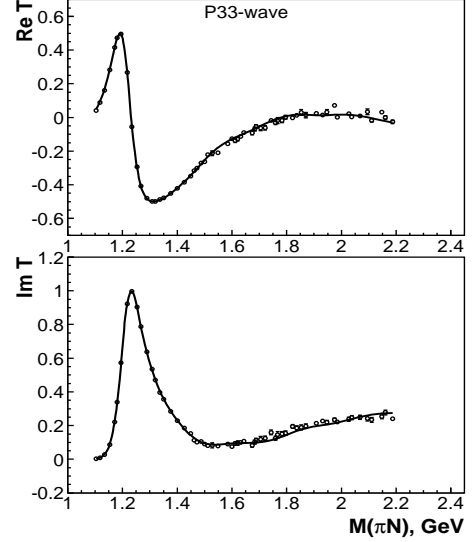


Fig. 18. Description of the P_{33} elastic amplitude extracted by SAID from the energy-independent partial wave analysis. The full curve shows our solution BG2010-02.

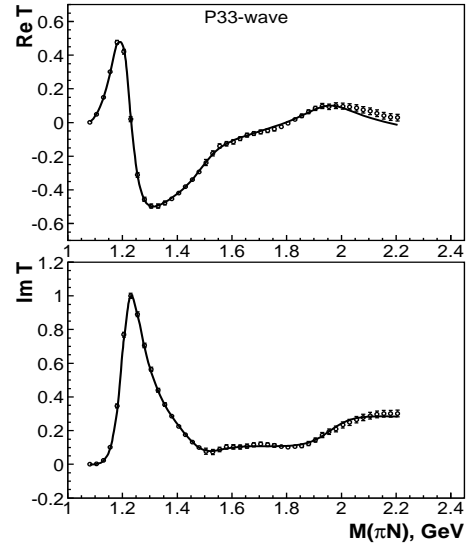


Fig. 19. Fit of Höhler's solution for the P_{33} elastic wave. For the fit we introduced 2% errors for Höhler's values below 1500 MeV and 5% errors above. The full curve shows our modified solution BG2010-02.

3.2 $(I)J^P = (3/2)1/2^+$

The P_{31} partial wave provides only a rather broad contribution to the $\pi^+p \rightarrow K^+\Sigma^+$ reaction with a maximum around 2 GeV. Moreover, we found a very small photoproduction contribution from this wave. First we tried a fit with a two-pole K-matrix parameterization: one pole in the 1600 MeV region and second one in the 2000 MeV region. In the best fit the poles are optimized at $1480 - i90$ and $1890 - i220$ MeV. The second pole is needed to reproduce the data, and we have no doubts that it exists. The position of the first pole is not well defined by the data, the corresponding K-matrix pole has very large couplings to the two-pion decay channels. If the pole is taken out of the fit and replaced by non-resonant terms for direct two-pion production, we do not observe a notable change in the quality of the data description. Thus we conclude that the present data base does not provide a proof for the existence of a state with $(I)J^P = (3/2)1/2^+$ quantum numbers in the 1500-1800 MeV mass region. The final solution was obtained with one K-matrix pole around 1900 MeV.

3.3 $(I)J^P = (1/2)3/2^+$

The existence of the four-star $N(1720)P_{13}$ resonance is, of course, beyond doubt and absolutely required in our fits. Its properties, in particular its $N\eta$ coupling, are controversial. At about the same mass, $N(1710)P_{11}$ can decay into the same final states, and the assignment of decays to one resonance or to the other one can be ambiguous.

This is, in particular, true for their $N\eta$ decays. In [184, 190], we obtained a better fit to the reaction $\gamma p \rightarrow p\eta$ when $N(1720)P_{13}$ was introduced as intermediate resonance than by using $N(1710)P_{11}$. This was in contrast to the results reported in [9, 139, 175] who assigned most of the $N\eta$ intensity to $N(1720)P_{13}$ but consistent with [191].

In the present analysis, data on $\pi^-p \rightarrow \eta n$ are included. The increase in data base now allows us to have contributions from both, $N(1710)P_{11}$ and $N(1720)P_{13}$, in the fit without running into fit instabilities. The $\pi^-p \rightarrow \eta n$ data exclude the large $N(1720)P_{13} \rightarrow \eta N$ coupling found in [184] (see Fig. 11). We confirmed, however, when this data are excluded and only one resonance is admitted, a preference for $N(1720)P_{13}$. The present data sets still do not yield an unambiguous answer for the $N\eta$ branching ratios. The ambiguity will be discussed below. In any case, the example shows the merits of using a large body of data in a coupled-channel analysis but also that ambiguities can still survive. In particular for such sensitive questions how much intensity one has to assign to specific states, the forthcoming double polarization data on π and η photoproduction are indispensable.

The $N(1900)P_{13}$ resonance was first introduced in our analysis [11]. It was required to achieve a good description of the double polarization observables C_x , C_z [116] in photoproduction of kaon-hyperon final states. The solution predicted very well the data on further double polarization observables, O_x , O_z , reported one year later [115].

$N(1900)P_{13}$ provides one of the dominant contributions to the $\gamma p \rightarrow K\Lambda$ and a notable contribution to the $\gamma p \rightarrow K^+\Sigma^0$ total cross sections. In the $\pi N \rightarrow K\Lambda$ reaction the P_{13} partial

wave has a clear peak around 1900 MeV. If the $P_{13}(1900)$ state is excluded from the fit, the χ^2 deteriorates significantly. Fig. 20 shows a few examples. The χ^2 change from the four figures is 110, the total χ^2 change 6179. We consider the existence of $N(1900)P_{13}$ to be solidly confirmed by the present analysis; splitting into two resonances is a likely possibility.

A mass scan of the P_{13} wave in the 1.75-2.1 GeV mass region for selected reactions is shown in Fig. 21. For the mass scan, the P_{13} amplitude was given by one K-matrix pole representing $N(1720)P_{13}$; above 1.75 GeV the amplitude was parameterized as Breit-Wigner amplitude. The mass was then increased in steps, all other variables were refitted. All mass scans have a clear minimum in the region 1900-2050 MeV, but the behavior of the curve is more complicated than that expected for a single pole. Some minima suggest a resonance mass of about 1900 MeV, others seem to prefer 2000 MeV. Hence we tried fits with a 3-pole 8-channel K-matrix. The fit produces the rather complicated structure in the region 1900 MeV and produced two close-by poles. The first pole is very stable and has a position close to the one reported in [11]. It has an appreciable coupling to the γp channel (see Table 8). The second pole is broader and higher in mass. In most solutions it has very small helicity couplings and thus decouples from the photoproduction data. The overall χ^2 change is significant: $\Delta\chi^2 = 6179$ when both resonances are removed and $\Delta\chi^2 = 2451$ when only one P_{13} resonance is removed. There is a possibility that a more flexible parameterization of the P_{13} partial wave can resolve this problem and describe all data with a single pole. However, at present, this double pole structure is needed to achieve a good description of all data. Thus we claim that there are indications for the existence of two close-by states even though the evidence for a double-pole structure is certainly not yet conclusive. The introduction of a fourth K-matrix pole in the region 2100-2300 MeV does not change the picture of the singularities in the 1900 MeV region.

The presence of pole singularities above 1700 MeV is not in conflict with the SAID energy-independent partial wave analysis of the elastic data: our description of the P_{13} partial wave is shown in Fig. 22. Höhler's result for the P_{13} wave, shown in Fig. 23, has no clear structure above 1800 MeV neither. We would like to mention that Höhler's result is appreciably different from the SAID result in the region 1700 MeV: it shows a much narrower structure. The substitution of the SAID amplitude by Höhler's amplitude thus leads to a narrower $N(1720)P_{13}$ state and a better definition of the singularities around 1900 MeV. For the fit using Höhler's solution we found helicity couplings and amplitudes residues for $N(1900)P_{13}$ to be larger than in the fit to the SAID amplitudes. Hence we increased the final errors in these quantities. Other partial waves were changed very little and the corresponding values are included in the errors.

The position in the complex plane and the amplitude residues for the two highest P_{13} poles are given in Table 8. In some of our solutions the $N(1720)P_{13}$ state has a large coupling to the S -wave $N(1520)D_{13}\pi$ channel which opens fast at the resonance position. As the result, we observe in different Riemann sheets a two-pole Flatté-like structure. For both these poles the closest physical region is at the $N(1520)D_{13}\pi$ threshold and the information extracted from residues of the pole on one sheet can be misleading. However, in most solutions the coupling to

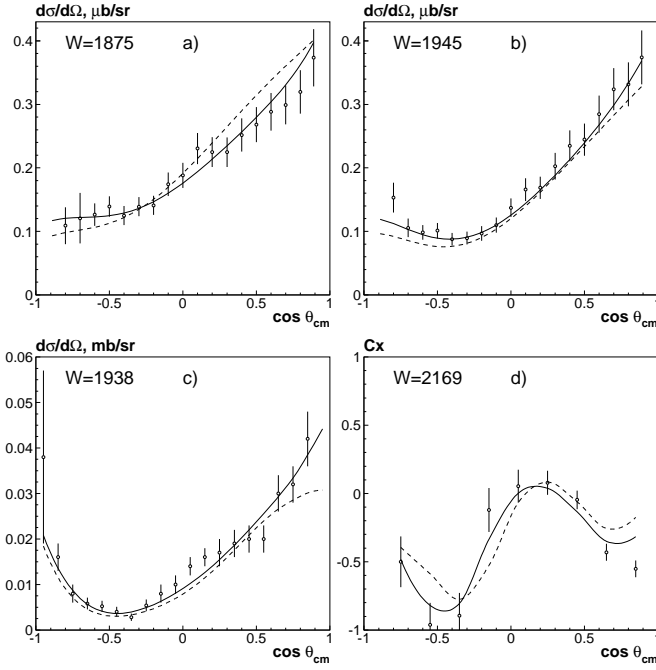


Fig. 20. Differential cross sections for $\gamma p \rightarrow K^+ \Lambda$ (a,b) and $\pi^- p \rightarrow K^0 \Lambda$ (c). C_x for $\gamma p \rightarrow K^+ \Lambda$. The full curve corresponds to the solution BG2010-02 with two close-by P_{13} states above $N(1720)P_{13}$, the dashed curve to a solution with the high-mass P_{13} resonances removed. The data shown contribute only a small fraction of the total χ^2 improvement (Table 10). For the two hypotheses, solution BG2010-02 yields, respectively: a) $\chi^2 = 8.3 / 24$ for 18 data points, b) $\chi^2 = 8.6 / 28$ for 18 data points, c) $17 / 33$ for 19 data points, and d) $22 / 60$ for 9 data points.

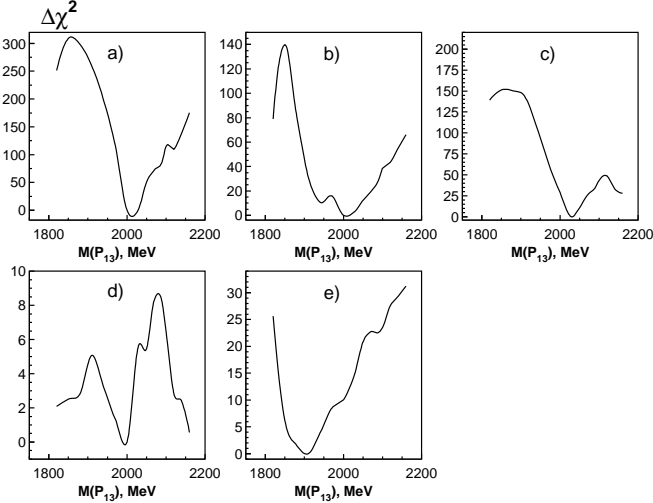


Fig. 21. Mass scan of the P_{13} Breit-Wigner amplitude. Change of χ^2 for the fit of a) differential cross sections (DCS) for $\gamma p \rightarrow K^+ \Lambda$ [112], b) DCS for $\gamma p \rightarrow p\eta$ [109], c) C_x, C_z for $\gamma p \rightarrow K\Lambda$ [116], d) C_x, C_z for $\gamma p \rightarrow K\Sigma$ [116], e) P for $\pi^- p \rightarrow K^0 \Lambda$ [21,22].

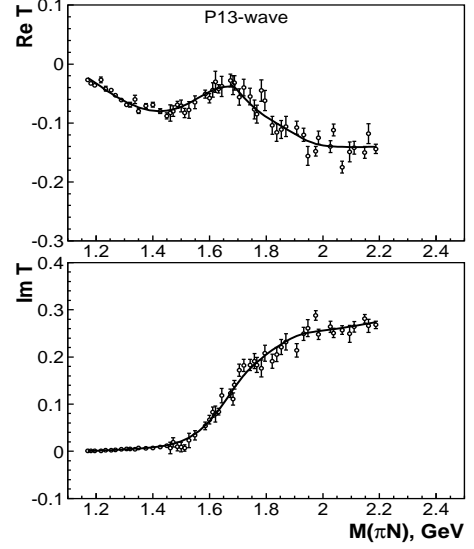


Fig. 22. Description of the P_{13} elastic amplitude (solution BG2010-02) extracted by SAID from the energy-independent partial wave analysis.

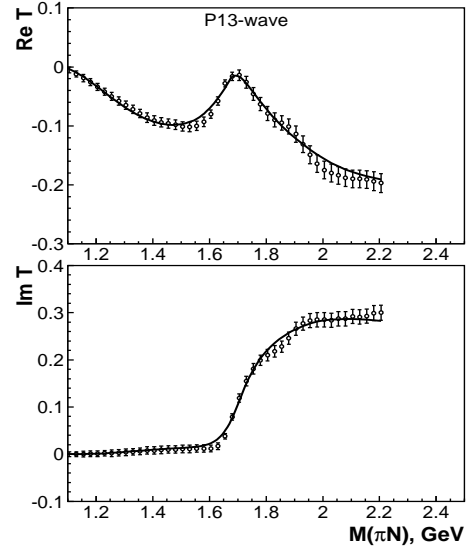


Fig. 23. Fit of Höhler's solution for the P_{13} elastic wave. For the fit of we introduced 2% errors for Höhler's values below 1750 MeV and 5% errors above. The curve shows the modified solution BG2010-02.

$N(1520)D_{13}\pi$ is smaller and residues from the pole closest to the physical region provide the characteristics of this state. These values are given in Table 9.

3.4 $(I)J^P = (1/2)1/2^+$

The P_{11} wave has a maximum in the $\pi^- p \rightarrow K^0 \Lambda$ reaction at 1720 MeV which suggests a contribution from the $N(1710)P_{11}$ state, the long tail may indicate the need for a further state at even higher mass. We therefore used a 4-pole K-matrix amplitude to fit the data: a first pole at the nucleon mass as Born

term, the well known Roper resonance at 1440 MeV, and two further poles.

One pole was found at $1690 \pm 25 - i110 \pm 15$ MeV which we identify with $N(1710)P_{11}$ and a second pole representing $N_{1/2+}(1875)$, a resonance which was first suggested in [120]. If both resonances are omitted from the fit, the contributions from the P_{11} wave to $\pi^- p \rightarrow K^0 \Lambda$ and $\pi^- p \rightarrow K^0 \Sigma$ become smaller and featureless, and the fit does not reproduce well the differential cross section (Fig. 24a,b) and exhibits problems with the description of the recoil asymmetry (Fig. 24c-f).

The description improves when $N(1710)P_{11}$ is introduced but the fit also demands the presence of a further pole in the 1870 MeV region: the interference of this state with the $N(1710)P_{11}$ resonance provides a correct energy dependence for this partial wave. The visible effect of this additional resonance in the individual plots are small but the overall improvement in χ^2 is significant (Table 10). As mentioned above, there are two equivalent solutions here. In the first solution, $N_{1/2+}(1875)$ is a rather narrow state with a small coupling to the πN channel and a rather small helicity coupling. In the second solution this state has appreciable πN and helicity couplings. In both solutions the hadron couplings for the $N(1710)P_{11}$ state are found to be very similar, however the helicity coupling differs in sign.

Fig. 24 shows the differential cross section, the observable $P d\sigma/(d\Omega \sin \Theta)$, and the Λ recoil polarization for $\gamma p \rightarrow K \Lambda$ for selected bins in the region 1720-1900 MeV. The solid curve represents our full fit with two P_{11} states above the Roper resonance, the dashed curve a fit with both these P_{11} states removed from the fit and when only non-resonant terms were admitted. The fit with only one P_{11} state in the region 1600-2000 MeV produced a pole close to the $P_{11}(1710)$ state. Such a fit has a systematically worse description in a large number of fitted reactions and in some places, there are visible systematical deviations (see Fig. 25). The inclusion of a third pole at 2100 MeV does not yield a visible effect.

To check stability of the poles we have introduced an additional P_{11} state in the higher mass region, first as a Breit-Wigner state and then as fifth K-matrix pole. Both Breit-Wigner and K-matrix amplitudes produced a compatible result with a pole at a mass around 2100 MeV and a rather large width of about 500 MeV. Although this state provides some improvement for the overall description of the data it also introduces a convergence problem to the fit. So, this state, if it exists, should be confirmed by other data, e.g. by double polarization data and/or data on multi-meson final states. Nevertheless, the state could be the resonance suggested by Höhler [1] and by Cutkosky [2].

Our conclusions concerning the existence of two P_{11} states above the Roper resonance are fully compatible with the data on elastic scattering, with the data from the analysis of Höhler and collaborators [1] as well as with the data from the analysis from Arndt and collaborators [3]. Figure 26 shows the comparison of the real and imaginary parts of our P_{11} elastic amplitude with the energy-independent analysis from [3]. In some solutions the fit shows a slight structure above the Roper resonance which arises from the combined analysis of the elastic and inelastic data. However a smooth behavior of elastic amplitude is also compatible with existence of resonances above Roper. The result of our analysis is hardly affected if we substitute the

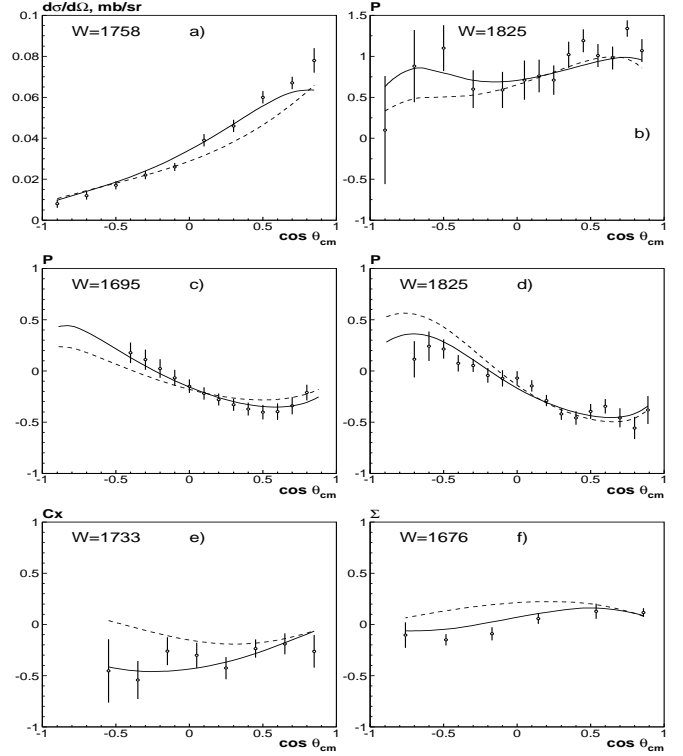


Fig. 24. a) Differential cross section and b) the Λ recoil polarization [21, 22] for $\pi^- p \rightarrow K^0 \Lambda$ [112] for four selected energy bins. c, d) Recoil polarization [112], e) C_x [112] and f) beam asymmetry Σ [114] for $\gamma p \rightarrow K^+ \Lambda$. The full curve corresponds to the solution BG2010-02 with two P_{11} states above the Roper resonance, the dashed curve to a solution with both P_{11} resonances removed.

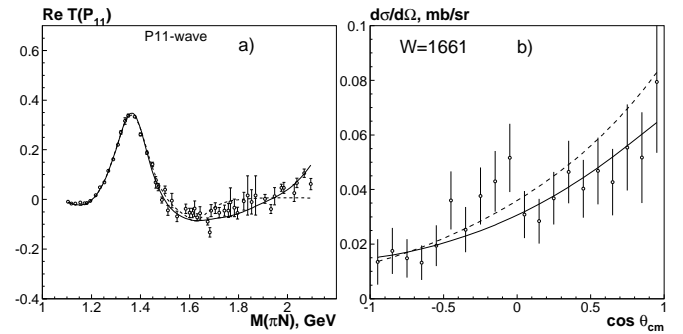


Fig. 25. a) Real part of the elastic P_{11} amplitude and b) the differential cross section [20] for $\pi^- p \rightarrow K^0 \Lambda$. The full curve corresponds to the solution BG2010-02 with two P_{11} states above the Roper resonance, the dashed curve to a solution with $N(1710)P_{11}$ removed.

SAID amplitudes by those of Höhler [1]. The only change in this solution are larger πN coupling constants of the two high-mass P_{11} resonances. We use the πN coupling constants from the two analyses to define the final errors. The data of Höhler and our fit are shown in Fig. 27. Höhler's data are given without errors. We use 2% errors below 1600 MeV and 5% errors above 1600 MeV

We performed a mass scan of the P_{11} wave in the 1.55-2.10 GeV mass region. In this case the P_{11} wave was parameterized as two pole K-matrix (nucleon pole and Roper resonance) and one relativistic multi-channel Breit-Wigner amplitude. This amplitude gave the best χ^2 for a Breit-Wigner mass at 1690 MeV and for 300 MeV width. Then, the mass of the Breit-Wigner amplitude was changed in 30 MeV steps, fixed, and all other parameters refitted. The χ^2 changes for 6 reactions with significant contributions from P_{11} partial wave are shown in Fig. 28. All curves have a clear minimum in the region 1670-1700 MeV, including the fit to $\gamma p \rightarrow K\Lambda$ [112]. To emphasize the need for a forth P_{11} resonance we have split the differential cross section on $\pi^- p \rightarrow K^0 \Lambda$ into a low energy region (below 1750 MeV) from [20], and the high-energy part (above 1750 MeV) from [21,22]. The low-energy region exhibits a clear minimum at about 1730 MeV; the high-energy part still “sees” the low-mass peak (now at 1650 MeV) but a second minimum in the region 1850-1880 MeV is clearly present.

In Table 11 we collect elastic pole residues of those resonances where our results can be compared with PDG values. In most cases, the agreement is excellent. Only for $\Delta(1920)P_{33}$ we find an opposite sign, and there are significant differences for $N(1710)P_{11}$ in the two solutions BG2010-01 and BG2010-02.

4 Extraction of the Breit-Wigner parameters

The dynamical Breit-Wigner parameterization of the πN elastic amplitude can be written as:

$$A_{BW} = \frac{(g_{\pi N}^{BW})^2 \rho_{\pi N}(s)}{M_{BW}^2 - s - i \sum_i (g_i^{BW})^2 \rho_i(s)}. \quad (16)$$

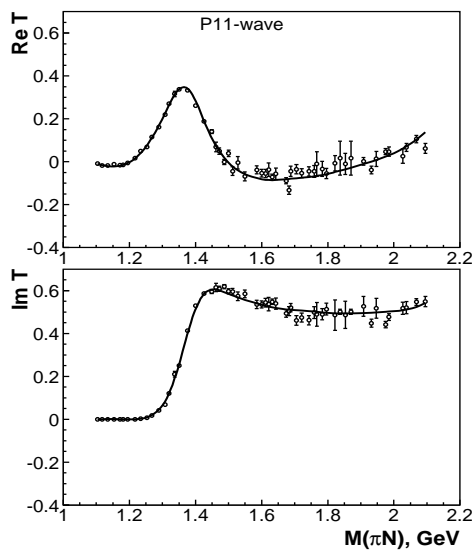


Fig. 26. The P_{11} elastic amplitude extracted by SAID in an energy independent partial wave analysis [3] and our energy-dependent fit (BG2010-02 solution).

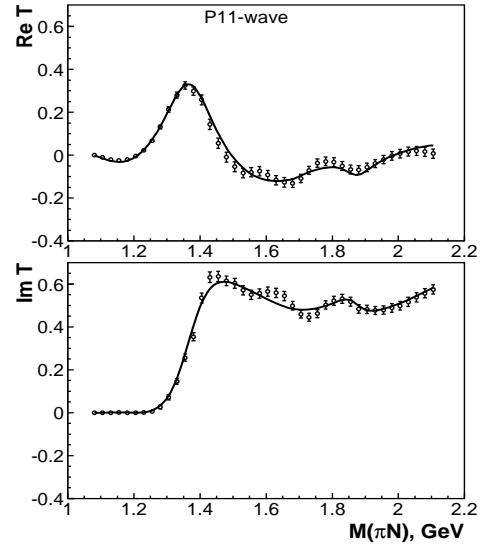


Fig. 27. The P_{11} elastic amplitude extracted by Höhler in an energy independent partial wave analysis [1] and our energy-dependent fit (modified BG2010-02). The Höhler result is shown as points with 2% errors below 1500 MeV and 5% above.

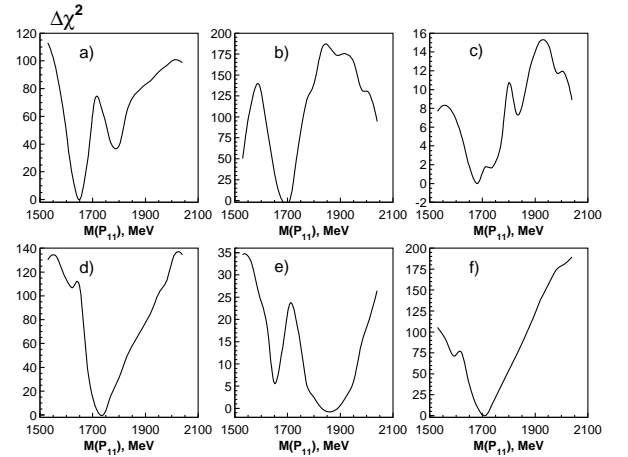


Fig. 28. Mass scan of the P_{11} Breit-Wigner amplitude. The P_{11} wave was parameterized as two pole K-matrix (nucleon pole and Roper resonance) plus one Breit-Wigner resonance. Change of χ^2 for the fit of a) differential cross section and b) the recoil asymmetry for $\gamma p \rightarrow K\Lambda$ [112], c) of the differential cross section for the $\pi^- p \rightarrow \eta n$ [18], of the differential cross section for the $\pi^- p \rightarrow K\Lambda$, separated into low-energy d) [20] and high-energy e) region [21,22], f) recoil asymmetry for $\pi^- p \rightarrow K^0 \Lambda$ [21,22].

Here s is the invariant energy squared, g_i^{BW} is the Breit-Wigner coupling and $\rho_i(s)$ is the phase volume for the channel i .

The expressions for the phase volumes $\rho_i(s)$ are given in [183]. To extract the Breit-Wigner parameters from the multi-channel multi-pole K-matrix parameterization we introduced the following procedure:

First, Breit-Wigner couplings g_i^{BW} were introduced which are proportional to the couplings calculated as residues in the pole (see Table 8):

$$g_i^{BW} = f g_i \quad (17)$$

Table 11. Elastic pole residues and comparison with PDG values.

$N(1440)P_{11}$	47 ± 3	$-(83 \pm 10)^\circ$	This work
	38	-98°	[3]
	40		[192]
	52 ± 5	$-(100 \pm 35)^\circ$	[2]
$N(1710)P_{11}$	5 ± 4	$-(80 \pm 40)^\circ$	BG2010-01
	7 ± 3	$-(190 \pm 25)^\circ$	BG2010-02
	15		[192]
	8	-167°	[2]
$N(1720)P_{13}$	22 ± 5	$-(85 \pm 20)^\circ$	BG2010-01
	28 ± 6	$-(85 \pm 20)^\circ$	BG2010-02
	25	-94°	[3]
	15		[192]
	8 ± 2	$-(160 \pm 30)^\circ$	[2]
$\Delta(1232)P_{33}$	51.4 ± 0.5	$-(47 \pm 1)^\circ$	This work
	52	-47°	[3]
	50	-48°	[192]
	52 ± 5	-47°	[2]
$\Delta(1600)P_{33}$	14 ± 3	$-(170 \pm 15)^\circ$	This work
	44	-147°	[3]
	17 ± 4	$-(150 \pm 30)^\circ$	[2]
$\Delta(1910)P_{31}$	38 ± 8	$-(120 \pm 15)^\circ$	This work
	38		[192]
	20 ± 4	$-(90 \pm 30)^\circ$	[2]
$\Delta(1920)P_{33}$	10 ± 6	$(20 \pm 60)^\circ$	This work
	24 ± 4	$-(150 \pm 30)^\circ$	[2]

where f is a global scaling factor for all decay channels. This factor as well as the Breit-Wigner mass are chosen to match the Breit-Wigner pole and the pole of the full amplitude resulting from the fit. Then, helicity Breit-Wigner couplings were calculated to reproduce the helicity residues in the pole position. Yet, in the case of rapidly increasing phase volumes, the Breit-Wigner mass and width are not easily compared with results of other analyses. Therefore we also introduced an effective Breit-Wigner mass which corresponds to the maximum of the squared $\pi N \rightarrow \text{final state}$ transition amplitude, and an effective width which corresponds to the full width half maximum of the squared-amplitude distribution. Further, we report the absolute value of the amplitude at the value of the effective mass. In the case of a simple Breit-Wigner amplitude, these numbers correspond to the mass, width and square root of the product of initial- and final-state branching ratios. The corresponding numbers for the P -wave resonances are given in Table 12-14. The effective mass can be well above the true pole position, in particular in final states with a rapidly increasing phase volume.

5 Discussion and conclusions

The classical path to explore nucleon and Δ resonances is the energy-independent partial wave analysis of elastic πN scattering data. The stakes are high: for a full reconstruction of the scattering amplitudes, required are high-precision data – over the full energy range and with complete angular coverage – (i) on differential cross sections, (ii) on the angular asymme-

Table 12. Effective masses, widths (in MeV) and $|(\Gamma_i \Gamma_f)^{\frac{1}{2}} / \Gamma_{tot}|$ calculated at the effective mass and given in percents.

$P_{11}(1440)$			
Channel	M_{eff}	Γ_{eff}	$ (\Gamma_i \Gamma_f)^{\frac{1}{2}} / \Gamma_{tot} $
$\pi N \rightarrow \pi N$	1389 ± 6	197 ± 10	$70 \pm 4\%$
$\pi N \rightarrow \eta N$	1612 ± 5	420 ± 25	$5 \pm 3\%$
$N_{3/2+}(1975)$			
Channel	M_{eff}	Γ_{eff}	$ (\Gamma_i \Gamma_f)^{\frac{1}{2}} / \Gamma_{tot} $
$\pi N \rightarrow \pi N$	1960 ± 20	220 ± 50	$1 \pm 1\%$
$\pi N \rightarrow \eta N$	1970 ± 20	220 ± 50	$3 \pm 2\%$
$\pi N \rightarrow K \Lambda$	1970 ± 20	220 ± 50	$4 \pm 2\%$
$\pi N \rightarrow K \Sigma$	1975 ± 20	210 ± 50	$1.5 \pm 1\%$
$N(1900)P_{13}$			
Channel	M_{eff}	Γ_{eff}	$ (\Gamma_i \Gamma_f)^{\frac{1}{2}} / \Gamma_{tot} $
$\pi N \rightarrow \pi N$	1900 ± 20	310 ± 70	$1.5 \pm 1\%$
$\pi N \rightarrow \eta N$	1910 ± 15	305 ± 70	$2 \pm 1\%$
$\pi N \rightarrow K \Lambda$	1910 ± 15	280 ± 70	$3.5 \pm 1.5\%$
$\pi N \rightarrow K \Sigma$	1920 ± 15	280 ± 70	$2.5 \pm 1\%$
$\Delta(1910)P_{31}$			
Channel	M_{eff}	Γ_{eff}	$ (\Gamma_i \Gamma_f)^{\frac{1}{2}} / \Gamma_{tot} $
$\pi N \rightarrow \pi N$	1895 ± 25	460 ± 40	$17 \pm 3\%$
$\pi N \rightarrow K \Sigma$	1950 ± 25	390 ± 30	$4 \pm 1\%$
$\Delta(1232)P_{33}$			
Channel	M_{eff}	Γ_{eff}	$ (\Gamma_i \Gamma_f)^{\frac{1}{2}} / \Gamma_{tot} $
$\pi N \rightarrow \pi N$	1229 ± 3	98^{+4}_{-6}	100%
$\Delta(1600)P_{33}$			
Channel	M_{eff}	Γ_{eff}	$ (\Gamma_i \Gamma_f)^{\frac{1}{2}} / \Gamma_{tot} $
$\pi N \rightarrow \pi N$	1500 ± 20	240^{+15}_{-40}	$15 \pm 3\%$
$\Delta(1920)P_{33}$			
Channel	M_{eff}	Γ_{eff}	$ (\Gamma_i \Gamma_f)^{\frac{1}{2}} / \Gamma_{tot} $
$\pi N \rightarrow \pi N$	1935 ± 35	310 ± 40	$7^{+6}_{-3}\%$
$\pi N \rightarrow K \Sigma$	1950 ± 20	280 ± 30	$4.5 \pm 2\%$

try of the outgoing pion when the target nucleon polarization is reversed, and (iii) on the polarization of the outgoing nucleon, again over the full energy range and with complete angular coverage.

These data do not exist. Hence one needs to rely on further theoretical input. Dispersion relations provide a powerful and flexible tool to constrain the low-energy region by our knowledge of strong interactions at high energies. However, approximations need to be made, and obviously, these approximations have a significant impact on the results. At least, the approximations made in the three classical energy-independent partial wave analyses [1,2,3] lead to significantly different amplitudes, at least in several partial waves and above the first resonance in a given partial wave.

Of course, energy-independent partial wave analyses are not the final step to determine the number and the properties of resonances in a particular partial wave. Real and imaginary part of the amplitude have to be fitted within an energy-dependent

Table 13. Effective masses, widths (in MeV) and $|(\Gamma_i \Gamma_f)^{\frac{1}{2}}/\Gamma_{tot}|$ calculated at the effective mass and given in percents for solution 01

$N(1710)P_{11}$			
Channel	M_{eff}	Γ_{eff}	$ (\Gamma_i \Gamma_f)^{\frac{1}{2}}/\Gamma_{tot} $
$\pi N \rightarrow \pi N$	1692 ± 5	200 ± 15	$4.5 \pm 2.5\%$
$\pi N \rightarrow \eta N$	1706 ± 5	200 ± 15	$3^{+2}_{-1}\%$
$\pi N \rightarrow K \Lambda$	1730 ± 6	205 ± 20	$8 \pm 3\%$
$N_{1/2+}(1875)$			
Channel	M_{eff}	Γ_{eff}	$ (\Gamma_i \Gamma_f)^{\frac{1}{2}}/\Gamma_{tot} $
$\pi N \rightarrow \pi N$	1859 ± 4	116 ± 15	$5 \pm 3\%$
$\pi N \rightarrow \eta N$	1860 ± 7	115 ± 15	$15^{+5}_{-2}\%$
$\pi N \rightarrow K \Lambda$	1862 ± 7	115 ± 15	$4 \pm 2\%$
$\pi N \rightarrow K \Sigma$	1864 ± 9	115 ± 15	$7 \pm 4\%$
$N(1720)P_{13}$			
Channel	M_{eff}	Γ_{eff}	$ (\Gamma_i \Gamma_f)^{\frac{1}{2}}/\Gamma_{tot} $
$\pi N \rightarrow \pi N$	1677^{+30}_{-10}	310 ± 30	$10 \pm 2\%$
$\pi N \rightarrow \eta N$	1700^{+40}_{-10}	300 ± 35	$7 \pm 3\%$
$\pi N \rightarrow K \Lambda$	1740 ± 25	410 ± 40	$3 \pm 2\%$
$\pi N \rightarrow K \Sigma$	1840 ± 25	480 ± 50	$8^{+5}_{-2}\%$

Table 14. Effective masses, widths (in MeV) and $|(\Gamma_i \Gamma_f)^{\frac{1}{2}}/\Gamma_{tot}|$ calculated at the effective mass and given in percents for solution 02

$N(1710)P_{11}$			
Channel	M_{eff}	Γ_{eff}	$ (\Gamma_i \Gamma_f)^{\frac{1}{2}}/\Gamma_{tot} $
$\pi N \rightarrow \pi N$	1700 ± 6	210 ± 20	$5 \pm 2\%$
$\pi N \rightarrow \eta N$	1714 ± 6	215 ± 20	$7 \pm 3\%$
$\pi N \rightarrow K \Lambda$	1740 ± 10	210 ± 20	$16 \pm 4\%$
$N_{1/2+}(1875)$			
Channel	M_{eff}	Γ_{eff}	$ (\Gamma_i \Gamma_f)^{\frac{1}{2}}/\Gamma_{tot} $
$\pi N \rightarrow \pi N$	1845 ± 25	340 ± 30	$8 \pm 4\%$
$\pi N \rightarrow \eta N$	1855 ± 30	320 ± 35	$9 \pm 3\%$
$\pi N \rightarrow K \Lambda$	1865 ± 30	330 ± 30	$10 \pm 4\%$
$\pi N \rightarrow K \Sigma$	1880 ± 30	300 ± 30	$6 \pm 2\%$
$N(1720)P_{13}$			
Channel	M_{eff}	Γ_{eff}	$ (\Gamma_i \Gamma_f)^{\frac{1}{2}}/\Gamma_{tot} $
$\pi N \rightarrow \pi N$	1660 ± 25	310 ± 30	$12 \pm 2\%$
$\pi N \rightarrow \eta N$	1690 ± 25	300 ± 30	$5 \pm 2\%$
$\pi N \rightarrow K \Lambda$	1730 ± 20	400 ± 35	$4 \pm 1\%$
$\pi N \rightarrow K \Sigma$	1840 ± 20	480 ± 40	$9 \pm 3\%$

model which parameterizes resonant and non-resonant terms. The model tries to describe the amplitudes with a minimum number of resonances; further resonances coupling weakly to $N\pi$ can always exist. But then, they have to show up in other reactions.

In the energy dependent analyses, the total number of nucleon and Δ resonances suggested by [1,2] is larger by more than a factor two than in [3]. In [3], more recent precision data were used and their predictions of the spin rotation parameters agree much better with recent data than those based on the am-

plitudes from [1,2]. Thus the existence of many states reported by PDG is seriously challenged.

The difference is very important for our understanding of the baryon spectrum. Quark models predict a large number of resonances in each partial wave. The high-mass resonances are predicted to have small couplings to $N\pi$, hence they may be difficult to identify in πN elastic scattering, but it is surprising when only one resonance is observed per partial wave. A modern view questions the usefulness of quarks to describe the nucleon excitation spectrum. Instead, resonances are generated dynamically from the interaction of baryons and mesons. In this approach, excitations above the lowest-mass state in a given partial wave are not necessarily expected. The results of [3] are thus a strong support for the conjecture that quark degrees of freedom may play only a minor role in the spectroscopy of light baryons. We just mention that a modern quark-model variant, AdS/QCD, provides a link between perturbative high-energy scattering and spectroscopy (see, e.g. [193] and references therein). In a special variant, AdS/QCD reproduces with surprising precision the full spectrum of nucleon and Δ resonances [194], including all those resonances which are challenged in [3]. If these all do not exist, the coincidence between AdS/QCD and data would be extremely fortuitous.

P -wave nucleon and Δ resonances provide a fruitful area in which the alternatives [1,2] and [3] can be tested. Above the famous $\Delta(1232)$, two further states, $\Delta(1600)P_{33}$ and $\Delta(1920)P_{33}$, were reported in [1,2]; $\Delta(1920)P_{33}$ is absent in [3]. There is no $N(1710)P_{11}$ above the Roper resonance in [3] and no $N(1900)P_{13}$. The four-star $\Delta(1910)P_{31}$ is required in [1,2], and is questionable in [3].

In this paper, we reported evidence for these debated states from a coupled-channel fit which includes inelastic reactions. We have studied the mass spectrum of P -wave nucleon and Δ resonances in a coupled-channel analysis of a large body of data on pion- and photo-induced reactions. Individual partial waves are typically described by 6-channel K-matrices with up to five poles. The coupled-channel fit minimizes the number of parameters needed to represent resonant and background contributions. The πN elastic amplitudes from energy-independent partial wave analyses are included in the data base. Hence we fit the same data as [1,3] but in our fits, the inelasticities are no black box but constrained by data from pion- and photo-induced inelastic reactions in which the final states are fully reconstructed. Particularly useful are here data on hyperon production. Λ and Σ baryons produced in a reaction reveal their polarization state in their decay. In recent experiments on photo-production of hyperons, polarized photons were used which allow the experiments to study the polarization transfer from the initial to the final state. These experiments are phase sensitive and constrain drastically the final solution. This use of inelastic reactions is, in our view, a major step forward compared to [1,3] since in the latter analyses, the inelasticities are not really under control.

The surprising result of our analysis is that the P -wave resonances reported by [1,2] and challenged by [3] are found with properties which are not very different from those reported by [1,2]. In particular we confirm existence and properties of $N(1710)P_{11}$ and $N(1900)P_{13}$ and of $\Delta(1600)P_{33}$ and $\Delta(1920)P_{33}$. We do not find evidence for $\Delta(1750)P_{31}$, a resonance not

seen by [1,2] (but in some other analyses) and, last not least, we confirm with good evidence $N_{1/2^+}(1875)$ [120,195] and find evidence for a tentative $N_{3/2^+}(1975)$.

Acknowledgements

We would like to thank the members of SFB/TR16 for continuous encouragement. We acknowledge financial support from the Deutsche Forschungsgemeinschaft (DFG) within the SFB/TR16 and from the Forschungszentrum Jülich within the FFE program.

References

1. G. Höhler, F. Kaiser, R. Koch and E. Pietarinen, "Handbook Of Pion Nucleon Scattering," Published by Fachinform. Zentr. Karlsruhe 1979, 440 P. (Physics Data, No.12-1 (1979)).
2. R. E. Cutkosky, C. P. Forsyth, J. B. Babcock, R. L. Kelly and R. E. Hendrick, "Pion - Nucleon Partial Wave Analysis," 4th Int. Conf. on Baryon Resonances, Toronto, Canada, Jul 14-16, 1980. Published in Baryon 1980:19 (QCD161:C45:1980)
3. R. A. Arndt, W. J. Briscoe, I. I. Strakovsky and R. L. Workman, Phys. Rev. C **74**, 045205 (2006)
4. E. Klempt and J. M. Richard, Rev. Mod. Phys. **82**, 1095 (2010).
5. R. A. Arndt, J. M. Ford and L. D. Roper, Phys. Rev. D **32**, 1085 (1985).
6. D. M. Manley and E. M. Saleski, Phys. Rev. D **45**, 4002 (1992).
7. C. Amsler *et al.*, Phys. Lett. B **667**, 1 (2008).
8. A. V. Anisovich, E. Klempt, V. A. Nikonov, M. A. Matveev, A. V. Sarantsev and U. Thoma, Eur. Phys. J. A **44**, 203 (2010).
9. T. P. Vrana, S. A. Dytman and T. S. H. Lee, Phys. Rept. **328**, 181 (2000).
10. N. Suzuki, B. Julia-Diaz, H. Kamano, T. S. Lee, A. Matsuyama and T. Sato, Phys. Rev. Lett. **104**, 042302 (2010) [arXiv:0909.1356 [nucl-th]].
11. V. A. Nikonov, A. V. Anisovich, E. Klempt, A. V. Sarantsev and U. Thoma, Phys. Lett. B **662**, 245 (2008).
12. G. Penner and U. Mosel, Phys. Rev. C **66**, 055212 (2002).
13. I. Horn *et al.*, Phys. Rev. Lett. **101**, 202002 (2008).
14. I. G. Alekseev *et al.*, Phys. Rev. C **55**, 2049 (1997).
15. I. G. Alekseev *et al.*, Phys. Lett. B **485**, 32 (2000).
16. I. G. Alekseev *et al.*, Eur. Phys. J. C **45**, 383 (2006).
17. I. G. Alekseev *et al.*, Eur. Phys. J. A **39**, 163 (2009).
18. W. B. Richards *et al.*, Phys. Rev. D **1**, 10 (1970).
19. S. Prakhov *et al.*, Phys. Rev. C **72**, 015203 (2005).
20. T. M. Knael *et al.*, Phys. Rev. D **11**, 1 (1975).
21. R. D. Baker *et al.*, Nucl. Phys. B **141**, 29 (1978).
22. D. H. Saxon *et al.*, Nucl. Phys. B **162**, 522 (1980).
23. K. W. Bell *et al.*, Nucl. Phys. B **222**, 389 (1983).
24. D. J. Candlin *et al.*, Nucl. Phys. B **226**, 1 (1983).
25. D. J. Candlin *et al.*, Nucl. Phys. B **311**, 613 (1989).
26. J. C. Hart *et al.*, Nucl. Phys. B **166**, 73 (1980).
27. S. Prakhov *et al.*, Phys. Rev. C **69**, 045202 (2004).
28. U. Thoma *et al.*, Phys. Lett. B **659**, 87 (2008).
29. A. V. Sarantsev *et al.*, Phys. Lett. B **659**, 94 (2008).
30. C. Weinheimer, Nucl. Phys. A **721** (2003) 781.
31. I. Horn *et al.*, Eur. Phys. J. A **38**, 173 (2008).
32. Y. Assafiri *et al.*, Phys. Rev. Lett. **90**, 222001 (2003).
33. E. Gutz *et al.*, Eur. Phys. J. A **35**, 291 (2008).
34. J. Ahrens *et al.*, Eur. Phys. J. A **34** 11, (2007).
35. M. Fuchs *et al.*, Phys. Lett. B **368**, 20 (1996).
36. J. Ahrens *et al.*, Phys. Rev. Lett. **88**, 232002 (2002).
37. J. Ahrens *et al.*, Eur. Phys. J. A **21**, 323 (2004).
38. O. Bartalini *et al.*, Eur. Phys. J. A **26**, 399 (2005).
39. O. Bartholomy *et al.*, Phys. Rev. Lett. **94**, 012003 (2005).
40. H. van Pee *et al.*, Eur. Phys. J. A **31**, 61 (2007).
41. M. Dugger *et al.*, Phys. Rev. C **76**, 025211 (2007).
42. G. Barbiellini *et al.*, Phys. Rev. **184**, 1402 (1969).
43. V. G. Gorbenko *et al.*, Pisma Zh. Eksp. Teor. Fiz. **19**, 659 (1974).
44. V. G. Gorbenko *et al.*, Yad. Fiz. **27**, 1204 (1978).
45. A. a. Belyaev *et al.*, Nucl. Phys. B **213**, 201 (1983).
46. G. Blanpied *et al.*, Phys. Rev. Lett. **69**, 1880 (1992).
47. R. Beck *et al.*, Phys. Rev. Lett. **78**, 606 (1997).
48. F. V. Adamian *et al.*, Phys. Rev. C **63**, 054606 (2001).
49. G. Blanpied *et al.*, Phys. Rev. C **64**, 025203 (2001).
50. N. Sparks *et al.*, Phys. Rev. C **81**, 065210 (2010).
51. P. S. L. Booth *et al.*, Nucl. Phys. B **121**, 45 (1977).
52. P. Feller *et al.*, Nucl. Phys. B **110**, 397 (1976).
53. V. G. Gorbenko *et al.*, Yad. Fiz. **26**, 320 (1977).
54. H. Herr *et al.*, Nucl. Phys. B **125**, 157 (1977).
55. M. Fukushima *et al.*, Nucl. Phys. B **136**, 189 (1978).
56. P. J. Bussey *et al.*, Nucl. Phys. B **154**, 492 (1979).
57. K. S. Agababian *et al.*, Sov. J. Nucl. Phys. **50**, 834 (1989) [Yad. Fiz. **50**, 1341 (1989)].
58. M. M. Asaturian *et al.*, JETP Lett. **44**, 341 (1986) [Pisma Zh. Eksp. Teor. Fiz. **44**, 266 (1986)].
59. A. Bock *et al.*, Phys. Rev. Lett. **81**, 534 (1998).
60. J. O. Maloy, Ph.D.Thesis, 1961.
61. V. G. Gorbenko *et al.*, Pisma Zh. Eksp. Teor. Fiz. **22**, 393 (1975).
62. S. Kato *et al.*, Nucl. Phys. B **168**, 1 (1980).
63. A. S. Bratashvsky *et al.*, Nucl. Phys. B **166**, 525 (1980).
64. A. S. Bratashvsky *et al.*, Ukr. Fiz. Zh. (Russ. Ed.) **31**, 1306 (1986).
65. P. J. Bussey *et al.*, Nucl. Phys. B **159**, 383 (1979).
66. J. Ahrens *et al.*, Eur. Phys. J. A **26**, 135 (2005).
67. R. O. Avakyan *et al.*, Sov. J. Nucl. Phys. **53**, 448 (1991) [Yad. Fiz. **53**, 717 (1991)].
68. S. D. Ecklund and R. L. Walker, Phys. Rev. **159**, 1195 (1967).
69. C. Betourne, J. C. Bizot, J. P. Perez-y-Jorba, D. Treille and W. Schmidt, Phys. Rev. **172**, 1343 (1968).
70. B. Bouquet *et al.*, Phys. Rev. Lett. **27**, 1244 (1971).
71. T. Fujii *et al.*, Phys. Rev. Lett. **26**, 1672 (1971).
72. K. Ekstrand *et al.*, Phys. Rev. D **6**, 1 (1972).
73. T. Fujii *et al.*, Nucl. Phys. B **120**, 395 (1977).
74. I. Arai *et al.*, J. Phys. Soc. Jap. **43**, 363 (1977).
75. E. J. Durwen, Ph.D. Thesis (1980); BONN-IR-80-7, Apr. 1980.
76. K. H. Althoff *et al.*, Z. Phys. C **18**, 199 (1983).
77. W. Heise, Ph.D. Thesis (1988); BONN-IR-88-06, Feb.1988.
78. K. Buechler *et al.*, Nucl. Phys. A **570**, 580 (1994).
79. H. W. Dannhausen *et al.*, Eur. Phys. J. A **11**, 441 (2001).
80. J. Ahrens *et al.*, Phys. Rev. C **74**, 045204 (2006).
81. M. Dugger *et al.*, Phys. Rev. C **79**, 065206 (2009).
82. R. E. Taylor and R. F. Mozley, Phys. Rev. **117**, 835 (1960).
83. R. C. Smith and R. F. Mozley, Phys. Rev. **130**, 2429 (1963).
84. J. Alspector *et al.*, Phys. Rev. Lett. **28**, 1403 (1972).
85. G. Knies *et al.*, Phys. Rev. D **10**, 2778 (1974).
86. V. B. Ganenko *et al.*, Yad. Fiz. **23**, 100 (1976).
87. P. J. Bussey *et al.*, Nucl. Phys. B **154**, 205 (1979).
88. V. A. Getman *et al.*, Nucl. Phys. B **188**, 397 (1981).
89. P. Hampe, Ph.D. Thesis, 1980.
90. R. Beck *et al.*, Phys. Rev. C **61**, 035204 (2000).
91. J. Ajaka *et al.*, Phys. Lett. B **475**, 372 (2000).
92. J. Bocquet *et al.*, AIP Conf. Proc. **603**, 499 (2001).

93. K. H. Althoff *et al.*, Nucl. Phys. B **53**, 9 (1973).
94. S. Arai *et al.*, Nucl. Phys. B **48**, 397 (1972).
95. P. Feller *et al.*, Phys. Lett. **52B**, 105 (1974) [Nucl. Phys. B **102**, 207 (1976)].
96. K. H. Althoff *et al.*, Phys. Lett. B **59**, 93 (1975).
97. H. Genzel *et al.*, Nucl. Phys. B **92**, 196 (1975).
98. K. H. Althoff *et al.*, Phys. Lett. B **63**, 107 (1976).
99. K. H. Althoff *et al.*, Nucl. Phys. B **131**, 1 (1977).
100. M. Fukushima *et al.*, Nucl. Phys. B **130**, 486 (1977).
101. V. A. Getman *et al.*, Yad. Fiz. **32**, 1008 (1980).
102. K. Fujii *et al.*, Nucl. Phys. B **197**, 365 (1982).
103. H. Dutz *et al.*, Nucl. Phys. A **601**, 319 (1996).
104. K. Egawa *et al.*, Nucl. Phys. B **188**, 11 (1981).
105. P. J. Bussey *et al.*, Nucl. Phys. B **169**, 403 (1980).
106. A. A. Belyaev *et al.*, Yad. Fiz. **40**, 133 (1984).
107. A. A. Belyaev *et al.*, Yad. Fiz. **43**, 1469 (1986).
108. B. Krusche *et al.*, Phys. Rev. Lett. **74**, 3736 (1995).
109. V. Crede *et al.*, Phys. Rev. C **80**, 055202 (2009).
110. J. Ajaka *et al.*, Phys. Rev. Lett. **81**, 1797 (1998).
111. O. Bartalini *et al.*, Eur. Phys. J. A **33**, 169 (2007).
112. M. E. McCracken *et al.*, Phys. Rev. C **81**, 025201 (2010).
113. R. G. T. Zegers *et al.*, Phys. Rev. Lett. **91**, 092001 (2003).
114. A. Lleres *et al.*, Eur. Phys. J. A **31**, 79 (2007).
115. A. Lleres *et al.*, Eur. Phys. J. A **39**, 149 (2009).
116. R. Bradford *et al.*, Phys. Rev. C **75**, 035205 (2007).
117. R. Bradford *et al.*, Phys. Rev. C **73**, 035202 (2006).
118. J. W. C. McNabb *et al.*, Phys. Rev. C **69**, 042201 (2004).
119. R. Lawall *et al.*, Eur. Phys. J. A **24**, 275 (2005).
120. R. Castelijns *et al.*, Eur. Phys. J. A **35**, 39 (2008).
121. R. L. Workman, R. A. Arndt and M. W. Paris, Phys. Rev. C **79**, 038201 (2009).
122. R. Arndt, W. Briscoe, I. Strakovsky and R. Workman, Eur. Phys. J. A **35**, 311 (2008).
123. R. Workman, R. A. Arndt and I. I. Strakovsky, Phys. Rev. C **62**, 048201 (2000).
124. R. A. Arndt, W. J. Briscoe, I. I. Strakovsky and R. L. Workman, Phys. Rev. C **66**, 055213 (2002).
125. Y. I. Azimov, R. A. Arndt, I. I. Strakovsky and R. L. Workman, Phys. Rev. C **68**, 045204 (2003).
126. R. A. Arndt, W. J. Briscoe, I. I. Strakovsky, R. L. Workman and M. M. Pavan, Phys. Rev. C **69**, 035213 (2004).
127. R. A. Arndt, W. J. Briscoe, I. I. Strakovsky and R. L. Workman, Phys. Rev. C **72**, 058203 (2005).
128. T. Mart and C. Bennhold, Phys. Rev. C **61**, 012201 (2000).
129. H. Haberzettl, C. Bennhold and T. Mart, Nucl. Phys. A **684**, 475 (2001).
130. K. Nakayama, Y. Oh and H. Haberzettl, Acta Phys. Polon. Supp. **2**, 23 (2009).
131. S. S. Kamalov, D. Drechsel, O. Hanstein, L. Tiator and S. N. Yang, Nucl. Phys. A **684**, 321 (2001).
132. S. S. Kamalov, L. Tiator, D. Drechsel, R. A. Arndt, C. Bennhold, I. I. Strakovsky and R. L. Workman, Phys. Rev. C **66**, 065206 (2002).
133. G. Y. Chen, S. Kamalov, S. N. Yang, D. Drechsel and L. Tiator, Nucl. Phys. A **723**, 447 (2003).
134. W. T. Chiang, S. N. Yang, L. Tiator, M. Vanderhaeghen and D. Drechsel, Phys. Rev. C **68**, 045202 (2003).
135. S. N. Yang, G. Y. Chen, S. S. Kamalov, D. Drechsel and L. Tiator, Nucl. Phys. A **721**, 401 (2003).
136. G. Y. Chen, S. S. Kamalov, S. N. Yang, D. Drechsel and L. Tiator, Phys. Rev. C **76**, 035206 (2007).
137. D. Drechsel, S. S. Kamalov and L. Tiator, Eur. Phys. J. A **34**, 69 (2007).
138. L. Tiator, S. S. Kamalov, S. Ceci, G. Y. Chen, D. Drechsel, A. Svarc and S. N. Yang, arXiv:1007.2126 [nucl-th].
139. M. Batinic, I. Slaus, A. Svarc and B. M. K. Nefkens, Phys. Rev. C **51**, 2310 (1995) [Erratum-ibid. C **57**, 1004 (1998)].
140. S. Ceci, A. Svarc and B. Zauner, Phys. Rev. Lett. **97**, 062002 (2006).
141. S. Ceci, A. Svarc, B. Zauner, M. Manley and S. Capstick, Phys. Lett. B **659**, 228 (2008).
142. S. Ceci, A. Svarc and B. Zauner, Phys. Rev. Lett. **102**, 209101 (2009).
143. S. Janssen, J. Ryckebusch, W. Van Nespen, D. Debruyne and T. Van Cauteren, Eur. Phys. J. A **11**, 105 (2001).
144. T. Corthals, D. G. Ireland, T. Van Cauteren and J. Ryckebusch, Phys. Rev. C **75**, 045204 (2007).
145. T. Corthals, T. Van Cauteren, P. Van Craeyveld, J. Ryckebusch and D. G. Ireland, Phys. Lett. B **656**, 186 (2007).
146. P. Vancraeyveld, L. De Cruz, J. Ryckebusch and T. Van Cauteren, Phys. Lett. B **681**, 428 (2009).
147. A. Y. Korchin, O. Scholten and R. G. E. Timmermans, Phys. Lett. B **438**, 1 (1998).
148. A. Usov and O. Scholten, Phys. Rev. C **72**, 025205 (2005).
149. A. Usov and O. Scholten, Phys. Rev. C **74**, 015205 (2006).
150. R. Shyam and O. Scholten, Phys. Rev. C **78**, 065201 (2008) [arXiv:0808.0632 [nucl-th]].
151. O. Scholten and A. Usov, Mod. Phys. Lett. A **23**, 2305 (2008).
152. R. A. Williams, C. R. Ji and S. R. Cotanch, Phys. Rev. C **46**, 1617 (1992).
153. J. C. David, C. Fayard, G. H. Lamot and B. Saghai, Phys. Rev. C **53**, 2613 (1996).
154. N. Kaiser, T. Waas and W. Weise, Nucl. Phys. A **612**, 297 (1997).
155. A. de la Puente, O. V. Maxwell and B. A. Raue, Phys. Rev. C **80**, 065205 (2009).
156. J. He and B. Saghai, Phys. Rev. C **80**, 015207 (2009).
157. T. S. H. Lee, Int. J. Mod. Phys. E **18**, 1215 (2009).
158. B. Julia-Diaz, T. S. Lee, A. Matsuyama and T. Sato, Phys. Rev. C **76**, 065201 (2007).
159. B. Julia-Diaz, T. S. Lee, A. Matsuyama, T. Sato and L. C. Smith, Phys. Rev. C **77**, 045205 (2008).
160. J. Durand, B. Julia-Diaz, T. S. Lee, B. Saghai and T. Sato, Phys. Rev. C **78**, 025204 (2008).
161. B. Julia-Diaz, B. Saghai, T. S. Lee and F. Tabakin, Phys. Rev. C **73**, 055204 (2006).
162. O. Krehl, C. Hanhart, S. Krewald and J. Speth, Phys. Rev. C **62**, 025207 (2000).
163. M. Doring, C. Hanhart, F. Huang, S. Krewald and U. G. Meissner, Nucl. Phys. A **829**, 170 (2009).
164. M. Doring, C. Hanhart, F. Huang, S. Krewald and U. G. Meissner, Phys. Lett. B **681**, 26 (2009).
165. M. Doring, C. Hanhart, F. Huang, S. Krewald, U. G. Meissner and D. Ronchen, arXiv:1009.3781 [nucl-th].
166. B. Borasoy, P. C. Bruns, U. G. Meissner and R. Nissler, Eur. Phys. J. A **34**, 161 (2007).
167. A. Sibirtsev, J. Haidenbauer, S. Krewald, T. S. H. Lee, U. G. H. Meissner and A. W. Thomas, Eur. Phys. J. A **34**, 49 (2007).
168. A. Sibirtsev, J. Haidenbauer, F. Huang, S. Krewald and U. G. Meissner, Eur. Phys. J. A **40**, 65 (2009).
169. F. Huang, A. Sibirtsev, J. Haidenbauer, S. Krewald and U. G. Meissner, Eur. Phys. J. A **44**, 81 (2010).
170. A. Sibirtsev, J. Haidenbauer, S. Krewald and U. G. Meissner, arXiv:1007.3140 [nucl-th].
171. F. K. Guo, C. Hanhart and U. G. Meissner, Phys. Lett. B **665**, 26 (2008).

172. T. Feuster and U. Mosel, Nucl. Phys. A **612**, 375 (1997).
173. T. Feuster and U. Mosel, Phys. Rev. C **58**, 457 (1998).
174. T. Feuster and U. Mosel, Phys. Rev. C **59**, 460 (1999).
175. G. Penner and U. Mosel, Phys. Rev. C **66**, 055211 (2002).
176. G. Penner and U. Mosel, Phys. Rev. C **66**, 055212 (2002).
177. V. Shklyar, H. Lenske, U. Mosel and G. Penner, Phys. Rev. C **71**, 055206 (2005) [Erratum-ibid. C **72**, 019903 (2005)].
178. V. Shklyar, G. Penner and U. Mosel, Eur. Phys. J. A **21**, 445 (2004).
179. V. Shklyar, H. Lenske and U. Mosel, Phys. Rev. C **72**, 015210 (2005).
180. V. Shklyar, H. Lenske and U. Mosel, Phys. Lett. B **650**, 172 (2007).
181. R. Shyam, O. Scholten and H. Lenske, Phys. Rev. C **81**, 015204 (2010).
182. A. Anisovich, E. Klempt, A. Sarantsev and U. Thoma, Eur. Phys. J. A **24** (2005) 111.
183. A. V. Anisovich and A. V. Sarantsev, Eur. Phys. J. A **30**, 427 (2006).
184. A. V. Anisovich, A. Sarantsev, O. Bartholomy, E. Klempt, V. A. Nikonov and U. Thoma, Eur. Phys. J. A **25**, 427 (2005).
185. W. Deinet, H. Mueller, D. Schmitt, H. M. Staudenmaier, S. Buniatov and E. Zavattini, Nucl. Phys. B **11**, 495 (1969).
186. R. M. Brown *et al.*, Nucl. Phys. B **153**, 89 (1979).
187. N. C. Debenham *et al.*, Phys. Rev. D **12**, 2545 (1975).
188. H. R. Crouch *et al.*, Phys. Rev. D **21**, 3023 (1980).
189. A. V. Sarantsev, V. A. Nikonov, A. V. Anisovich, E. Klempt and U. Thoma, Eur. Phys. J. A **25** (2005) 441.
190. O. Bartholomy *et al.*, Eur. Phys. J. A **33**, 133 (2007).
191. I. G. Aznauryan, Phys. Rev. C **68**, 065204 (2003).
192. G. Höhler, πN Newslett. **9**, 108 (1993).
193. S. J. Brodsky, G. F. de Teramond and A. Deur, Phys. Rev. D **81**, 096010 (2010).
194. H. Forkel and E. Klempt, Phys. Lett. B **679**, 77 (2009).
195. A. V. Anisovich, V. Kleber, E. Klempt, V. A. Nikonov, A. V. Sarantsev and U. Thoma, Eur. Phys. J. A **34**, 243 (2007).